ELUCIDATING THE CORRELATIONS BETWEEN POST-PROCESSING PARAMETERS AND MECHANICAL PROPERTIES OF 3D PRINTED COPPER COMPOSITE

BY

SYED FOUZAN IFTEKAR

A dissertation submitted in fulfilment of the requirement for the degree of Master of Science in Manufacturing Engineering

Kulliyyah of Engineering
International Islamic University Malaysia

OCTOBER 2023

ABSTRACT

3D printing is a promising technology with the potential to revolutionize the additive manufacturing industry. Recently, the application of metal-based 3D Printing has been widely used especially in the aerospace, medical, and automotive industry. However, the cost of such machines is expensive and thus restricts access to this technology for small and medium enterprises. Thus, moving from expensive Selective Laser Melting (SLM) to Fused Deposition Modeling (FDM) Technology is a good alternative. Currently, the greatest challenges in advancing a low-cost FDM Metal 3D printing technology are post-processing, parameters affecting the post processes, accuracy, mechanical properties and microstructure of the finished parts. This project aims to investigate the post-processing techniques for 3D printed copper composites using an FDM 3D printer. To achieve the aim of this research, a hardened steel nozzle designed for metal composite filaments was used. Post-processing steps included debinding and sintering to convert the copper polymer composite into pure metal. The research employed the Design of Experiments (DOE) approach, specifically the Taguchi method, for optimization. An L8 orthogonal test array was constructed to determine the optimized parameters for debinding and sintering holding times. The findings revealed that the debinding process significantly affected shrinkage and hardness. The samples exhibited an average shrinkage of 30.59%, except for two samples that turned into small pieces due to improper debinding holding time. The debinding and sintering parameters played a crucial role in the successful conversion of the copper polymer composite into pure metal. These findings contribute to making metal 3D printing more affordable and accessible, opening up opportunities in different industries and supporting sustainable manufacturing practices. In future research, it is important to work on improving the way researchers finish the 3D printed metal parts. This includes finding better ways to remove binders and fuse the metal particles together during post-processing. Researchers should also look into simplifying the post-processing steps and finding ways to print larger parts.

خلاصة البحث

تعد الطباعة ثلاثية الأبعاد تقنية واعدة لها القدرة على إحداث ثورة في صناعة المواد المضافة. في الآونة الأخيرة ، تم استخدام تطبيق الطباعة ثلاثية الأبعاد القائمة على المعدن على نطاق واسع خاصة في صناعة الطيران والطب وصناعة السيارات. ومع ذلك ، فإن تكلفة هذه الآلات باهظة الثمن وبالتالي تقيد الوصول إلى هذه التكنولوجيا للمؤسسات الصغيرة والمتوسطة. وبالتالي ، فإن الانتقال من تقنية النوبان الانتقائي ، يعد بديلاً جيدًا. حاليا (FDM) الباهظة الثمن إلى تقنية نمذجة الترسيب المنصهر (SLM) بالليزر منخفضة التكلفة في مرحلة ما بعد FDM Metal 3D تتمثل أكبر التحديات في تطوير تقنية طباعة المعالجة ، والمعلمات التي تؤثر على عمليات ما بعد ، والدقة ، والخصائص الميكانيكية ، والبنية الدقيقة للأجزاء النهائية. يهدف هذا المشروع إلى التحقيق في تقنيات ما بعد المعالجة لمركبات النحاس المطبوعة ثلاثية الأبعاد. لتحقيق هدف هذا البحث ، تم استخدام فوهة FDM ثلاثية الأبعاد باستخدام طابعة فولاذية صلبة مصممة للخيوط المعدنية المركبة. تضمنت خطوات المعالجة اللاحقة التجليخ والتلبيد لتحويل وتحديدًا ، (DOE) مركب البوليمر النحاسي إلى معدن نقي. استخدم البحث نهج تصميم التجارب لتحديد المعلمات L8 من أجل التحسين. تم إنشاء مصفوفة اختبار متعامدة ، Taguchi طريقة المحسَّنة لتصفية وتلبيد أوقات الاحتفاظ. أوضحت النتائج أن عملية التنقية أثرت بشكل كبير على الانكماش والصلابة. أظهرت العينات انكماشًا متوسطًا بنسبة 40٪ ، باستثناء عينتين تحولتا إلى قطع صغيرة بسبب وقت احتجاز غير مناسب للكسر. لعبت معاملات التنقية والتلبيد دورًا مهمًا في التحويل الناجح لمركب بوليمر النحاس إلى معدن نقي. تساهم هذه النتائج في جعل الطباعة المعدنية ثلاثية الأبعاد ميسورة التكلفة ويمكن الوصول إليها ، مما يفتح الفرص في مختلف الصناعات ويدعم ممارسات التصنيع المستدامة. في البحث المستقبلي ، من المهم العمل على تحسين الطريقةالباحث ننهي بها الأجزاء المعدنية المطبوعة ثلاثية الأبعاد. يتضمن ذلك إيجاد طرق أفضل لإزالة الروابط ودمج جزيئات المعدن معًا أثناء المعالجة اللاحقة. يجب على الباحثين أيضًا النظر في تبسيط خطوات ما بعد المعالجة وإيجاد طرق لطباعة أجزاء أكبر

APPROVAL PAGE

I certify that I have supervised and read this study and that in my opinion; it conforms to acceptable standards of scholarly presentation and is fully adequate, in scope and quality, as a thesis for the degree of Master of Science in Manufacturing Engineering.

……
Nor Aiman Sukindar
Supervisor

……
Adibah Amir
Co-Supervisor

……
Muhammad Hanafi Azami
Co-Supervisor

……
Abdul Aabid
Co-Supervisor

I certify that I have read this study and that in my opinion it conforms to acceptable standards of scholarly presentation and is fully adequate, in scope and quality, as a thesis for the degree of Master of Science in Manufacturing Engineering.

……
Shafie Kamaruddin
Internal Examiner 1

……
Yang Chuan Choong
Internal Examiner 2

This dissertation was submitted to the Department of Manufacturing and Materials Science Engineering and is accepted as a fulfillment of the requirement for the degree of Master of Science in Manufacturing Engineering.

……
Ahmad Zahirani Ahmad Azhar
Head, Department of
Manufacturing and Materials
Engineering

This dissertation was submitted to the Kulliyyah of Engineering and is accepted as fulfillment of the requirement for the degree of Master of Science in Manufacturing Engineering.

……
Sany Izan Ihsan
Dean, Kulliyah of Engineering

DECLARATION

I hereby declare that this thesis is the result of my own investigations, except where otherwise stated. I also declare that it has not been previously or concurrently submitted as a whole for any other degrees at IIUM or other institutions.

Syed Fouzan Iftekar

Signature ..... Date 26-07-2023

INTERNATIONAL ISLAMIC UNIVERSITY MALAYSIA

DECLARATION OF COPYRIGHT AND AFFIRMATION OF FAIR USE OF UNPUBLISHED RESEARCH

DEVELOPMENT OF MIMO DIVERSITY TECHNIQUE WITH DISCRETE WAVELET TRANSFORM FOR MILLIMETER WAVE COMMUNICATION SYSTEM

I declare that the copyright holders of this thesis are jointly owned by the student and IIUM.

By signing this form, I acknowledged that I have read and understand the IIUM Intellectual Property Right and Commercialization policy.

Affirmed by Syed Fouzan Iftekar

……..…….. 26-07-2023 ……..

Signature Date

ACKNOWLEDGEMENTS

All glory is due to Allah, the Almighty, whose Grace and Mercies have been with me throughout the duration of my programme. Although, it has been tasking, His Mercies and Blessings on me ease the herculean task of completing this thesis.

I am most indebted to my supervisor, Asst. Prof. Ir. Ts. Dr. Nor Aiman Bin Sukindar, whose enduring disposition, kindness, promptitude, thoroughness and friendship have facilitated the successful completion of my work. I put on record and appreciate his detailed comments, useful suggestions and inspiring queries which have considerably improved this thesis. I am also grateful to my co-supervisor, Dr. Adibah Binti Amir, whose support and cooperation contributed to the outcome of this work. Furthermore, I am humbled by the profound knowledge and valuable insights shared by the esteemed members of the Supervisory Committee, namely Associate Professor Dr. Abdul Aabid and Dr. Muhammad Hanafi Azami. Their constructive comments and innovative ideas have made a significant impact on the enhancement of this thesis, and I am deeply appreciative of their valuable contributions.

Lastly, my gratitude goes to my beloved wife, Heba Sayeed, for her prayers whose unwavering support, unwavering motivation, and unwavering strength have propelled me forward in the difficult path towards completing this thesis. Her constant belief in my abilities has been a wellspring of inspiration. Most certainly, it is with immense pleasure and deep gratitude that I also dedicate this work to my esteemed parents, my esteemed in-laws, and all members of my family. Their unwavering support, resolute faith, and unyielding belief in my capabilities have been an invaluable gift throughout this research. I express my sincere thanks to them for their enduring support and boundless patience, which have drove my determination to accomplish this goal.

Once again, we glorify Allah for His endless mercy on us one of which is enabling us to successfully round off the efforts of writing this thesis. Alhamdulillah

TABLE OF CONTENTS

LIST OF TABLES

LIST OF FIGURES

LIST OF ABBREVIATIONS

3D	Three Dimension
SLM	Selective Laser Melting
FDM	Fused Deposition Modeling
AM	Additive Manufacturing
CAD	Computer Aided Design
SLS	Selective Laser Sintering
LPBF	Laser Powder Bed Fusion
EBM	Electron Beam Melting
PLA	Polylactic Acid
ABS	Acrylonitrile Butadiene Styrene
EDX	Energy Dispersive X-Ray Spectroscopy
PBF	Powder Bed Fusion
CO2	Carbon Dioxide
TPU	Thermoplastic Polyurethane
PA6	Polyamide six
PA12	Polyamide twelve
DMLS	Direct Metal Laser Sintering
EB PBF	Electron Beam Powder Bed Fusion
ADAM	Atomic Diffusion Additive Manufacturing
FFF	Fused Filament Fabrication
Al	Aluminum
Cu	Copper
Fe	Iron
O	Oxygen
Ca	Calcium

Mg	Magnesium
MIG	Metal Inert Gas
GTAW	Gas Tungsten Arc Welding
NDT	Non-Destructive Testing
SEM	Scanning Electron Microscopy
DOE	Design of Experiments
RF	Radio Frequency
SED	Scanning Electron Microscopy Electron Detector
WD	Working Distance
HV	Vickers Hardness

CHAPTER ONE

INTRODUCTION

1.1 OVERVIEW

This introductory chapter lays down a foundation and discusses the background of this thesis, describes broadly the problem statement that this thesis will deal and from that identifies objectives to be solved detailed methodology is discussed at the end of this chapter.

1.2 BACKGROUND OF THE STUDY

3D printing or additive manufacturing (AM) is a group of technologies that are used to build prototypes, physical models and finished parts from three-dimensional (3D) computer-aided design (CAD) data. Studies showed that technology has developed rapidly since it is reshaping the manufacturing industry with foreseeable benefits including complex designs, greater structural efficiency, reduction in material consumption and wastage, enhanced customization, and improved accuracy and safety. There has been an increase in demand for metal prototypes and tools. The introduction of non-polymeric material, including metal, has been widely used in 3D printing applications. Subsequently, powder bed fusion is a specific 3D printing technique which uses high power-density laser to melt and fuse metallic powders such as Selective Laser Sintering (SLS), Laser Powder Bed Fusion (LPBF), Electron Beam Melting (EBM), and among these technologies SLS or SLM technology has the highest demand in the market. And a commercial example of Selective Laser Melting is a DMG Mori Lasertec 12 SLM 3D printer, a German-made 3D Printer with a cost of 2.3 million Ringgit. Therefore, such machines are too expensive and thus restrict access to this technology for small and medium enterprises. Another 3D printing technology that can print metal is a material extrusion technology which is subdivided into Fused Deposition Modelling (FDM), 3D Bioprinting, and Construction 3D Printing, and among these technologies Fused Deposition Modelling (FDM) technology has the highest demand in the market

as it is the most affordable technology in the market as it ranges from RM500 to RM30000 (Ramazani & Kami, 2022) .

The purpose of this research is to investigate to print metal in a low-cost Fused Deposition Modelling 3D printer with effective post-processing parameters by utilizing the novel ideas and resources of previous research. Currently, the primary metal 3D printing heat sources are lasers, electron beams and electric arcs. The research and applications of lasers in metal 3D printing are extensive; Laser heating produces high-precision parts with good internal structures and great mechanical properties. However, lasers and metal powders are expensive (Huang et al., 2023) but coming to Fused Deposition Modelling based on a previous study, the welding process was used in this method to build 3D parts for the first time where containers and useful shapes were produced. Similarly, a scholar had successfully developed a 3D structure using a rapid prototyping process with a combination of micro tungsten inert gas welding and a layered manufacturing method in an FDM 3D printer. The results showed that a 3D structure without mould for micro component metals with high strength and oxidization resistance can successfully be built. The research was carried out by Kumar Singh & Chauhan, (2016) where they enhanced a technique of printing metal in an FDM 3D printer by using an Induction furnace and ceramic nozzle with a Tungsten tip. But in all the above FDM 3D printing methods, the metal parts were printed with the lowest resolutions and couldn't make any use of such parts in printing prototypes or any industrial component due to lack of accuracy. Thus, implementing an alternative method to print Metal using a Fused Deposition Modelling 3D Printer. This research is anchored on the assumptions that adding a hardened steel nozzle to the Extruder using to melt the metal filament which is more affordable and simpler than using the Laser-Metal Wire Deposition method or Tungsten inert gas method. However, the Filament used to print is a polymer-metal which consists of pure Metal powder whereas the polymer material is made of Polylactic Acid and Binding agents such as Polyethylene Wax. This helps the filament to print as normally as PLA or ABS. But the disadvantage of polymer-metal filament is that it will break more easily due to its high metal content hence avoiding pull and friction requires the filament to come off the spool straight into the feeder which normalizes the printing process. Further, it requires post-processing by removing the polymer or binding agent from the printed part by the debinding method and then heating the remaining 3D printed pure metal part by Sintering method

to fuse the atomic particles and to attain higher tensile strength. As a result, we can utilize such precise and higher-resolution metal parts to print especially Orthopaedic implants on a simple desktop FDM 3D printer. And since additive manufacturing is envisioned as the future of manufacturing, our abundance of locally high-quality materials must be capitalized upon effectively. To be self-sustainable and technologically forward in the foreseeable future, researchers must invest in this technology. The significance of this research is to provide knowledge and establish curiosity and fascination towards the Aerospace industry among academic researchers in Malaysia contributing to the development of economic growth Malaysia needs "Big innovation purpose" to stay ahead, says its government agency creating jobs, and facilitating international trade and tourism in the country. Aerospace engineers are the key people for making the next step for humans to travel faster around the world and explore the technological capabilities of flying vehicles.

1.3 PROBLEM STATEMENT

Metal 3D printing is a promising technology for producing complex and high-performance parts for various applications, especially in the aerospace, medical prosthetics and Automobile industry. However, metal 3D printing using laser-based methods is very expensive and requires specialized equipment and materials. Therefore, researchers have explored alternative methods of metal 3D printing using fused deposition modelling (FDM) technology, which is more accessible and affordable. FDM metal 3D printing uses a metal-polymer filament that consists of 90% metal powder and 10% polymer binder. The printed part contains 90% of metal powder, which can be converted into pure metal by post-processing steps of debinding and sintering.

However, FDM metal 3D printing also faces some challenges, mainly related to the post-processing parameters. Debinding and sintering are critical steps for achieving the desired mechanical properties of the printed metal part, such as strength, ductility and density. However, if the post-processing parameters are not optimized, the printed metal part may suffer from defects such as cracks, unsintered regions, brittleness, complete melting of the part, and the inability to achieve the desired shape. Moreover,

the microstructure of the printed metal part may exhibit the presence of undesirable pores, which can affect its performance and reliability.

Therefore, this study aims to investigate the rheological characteristics of copper-based metal composites and examine how their processing and post-processing parameters affect their quality and performance. Copper-based metal composites are chosen because they have high electrical and thermal conductivity, corrosion resistance and mechanical strength, which make them suitable for various applications (Ambrus et al., 2021). The study will use FDM technology to print copper-based metal composites with different compositions and geometries. The study will also analyse the effects of different debinding and sintering parameters on the mechanical properties, microstructure and density of the printed metal parts. The study will provide insights into the optimal processing and post-processing conditions for FDM metal 3D printing and contribute to the advancement of this technology.

1.4 RESEARCH OBJECTIVE

The research aims to investigate the fabrication of metal using FDM 3D Printer with effective post-processing techniques. The objective is to conduct a quantitative study of literature and industry practices. Specifically, the study has the following objectives:

- To fabricate metal 3D printed samples by using the fused deposition modelling (FDM) technique.
- To identify the optimized holding time and temperature using the Taguchi method for post-processing of FDM printed metal parts in the debinding and sintering process with different layer thicknesses.
- To investigate the effects of post-processing parameters on the mechanical properties, dimensions, chemical composition and microstructure, of sintered copper composite parts.

1.5 SIGNIFICANCE OF RESEARCH

The research on Fused Deposition Modelling (FDM) metal 3D printing and its post-processing techniques is significant for several reasons. It aims to make metal 3D printing more accessible and affordable by overcoming the cost limitations of traditional methods. This opens up opportunities for small and medium enterprises and individuals to utilize this technology. Additionally, the research advances industrial applications, particularly in aerospace, medical prosthetics, and automotive industries, by improving the mechanical properties of FDM-printed metal parts. It optimizes post-processing parameters to enhance the quality and performance of the printed components. Furthermore, the research contributes to knowledge and stimulates further advancements in the field of metal additive manufacturing. It also has economic implications, fostering growth, innovation, and job creation, particularly in countries like Malaysia. Overall, this research drives progress in metal 3D printing, making it more accessible, efficient, and impactful across various industries.

1.6 SCOPE OF THE RESEARCH

The scope of this research study is to investigate the impact of post-processing techniques on the mechanical properties and dimensional accuracy of metal 3D printed samples using the Fused Deposition Modeling (FDM) method. The specific objectives include assessing the effects of sintering temperature on hardness and measuring the shrinkage percentages of printed samples after the sintering process. Additionally, the study aims to determine the presence of pores, diffusion of metal particles, and the chemical composition, particularly the percentage of copper, in the samples. The research will be conducted using a sample size of 8 printed samples, each measuring 25x25x5 mm. The study duration is set at 3 months, and the methodology encompasses Design of Experiments using the Taguchi method, sample preparation, printing process control using a standard FDM printer with predefined parameters, post-processing steps such as debinding and sintering at different temperatures ranging from 800°C to 1200°C with a constant heating rate and holding time, mechanical analysis using micrometers and Vickers hardness testing, and microstructure and chemical analysis using scanning electron microscopy and energy-dispersive X-ray spectroscopy (EDX). The scope

acknowledges the limitations of the sample size and duration, ensuring practicality and feasibility while providing valuable insights into the specified research parameters. The scope also excludes other post-processing techniques such as polishing or coating, other metal materials such as steel or aluminum, other printing methods such as selective laser melting or direct metal laser sintering, and other mechanical properties such as tensile strength or fatigue resistance.

1.7 THESIS OUTLINE

This thesis is organized into five chapters:

Chapter 1 – Chapter One introduces the background, problem statement, research objectives, significance, scope and organization of the study.

Chapter 2 – Chapter Two reviews the relevant literature on different types of 3D printer technologies, metal 3D printing, FDM metal 3D printing, filament used in metal FDM 3D printers, process parameters for 3D printing metal in FDM 3D printers, post-processing techniques for FDM metal parts, mechanical characterization and performance evaluation in FDM metal printing, and FDM metal 3D printing applications in aerospace, medical and automobile field.

Chapter 3 – Chapter Three describes the research methodology, including the research design and approach, materials and equipment, sample preparation, printing process, post-processing, mechanical analysis, microstructure and chemical analysis, and data collection and analysis methods.

Chapter 4 – Chapter Four presents the results and discussion of the experimental work, including the experimental setup, process parameter optimization, post-processing, mechanical properties analysis, microstructural characterization.

Chapter 5 – Chapter Five concludes the thesis with a summary of key findings and recommendations for future research

CHAPTER TWO

LITERATURE REVIEW

2.1 INTRODUCTION

As the global interest in the automation industry rises, researchers are rapidly investigating different ways to improve the Additive manufacturing technology. Various industries have incorporated 3D printers to simultaneously improve efficiency and customizability. So, an alternative method is found recently by some companies like Mark forge, virtual foundry, etc. and researchers have started further studies on this method where a metal polymer composite filament is used to fabricate using a low-cost desktop Fused Deposition Modelling 3D printer (Ramazani & Kami, 2022). This research investigates how copper-polymer composite can be fabricated using low cost FDM 3D printing technology with optimized post processing parameters.

2.2 IMPORTANCE OF METAL

Metals on the other hand are important for various reasons such as their durability, conductivity, and malleability, making them ideal for use in construction, electrical wiring, and manufacturing. They also have high melting and boiling points, which makes them useful for high-temperature applications. Metals are usually very strong, most durable and highly resistant to everyday wear and tear. As such, they have been used since ancient times for a lot of things. And even today with advances in technology and a lot of other things the uses of metals have broadened greatly. Metals even play a key role in the economy.

Metals are found in every substance or thing related to the modern world; from cars to the crockery, from Jewelry to the buildings, hence, everything that exists in this modern world has to an extent metal utilization. They are used extensively in manufacturing machines for industries, agriculture or farming and automobiles which include road vehicles, railways, Aero planes, rockets etc. Here, the commonly used metals are iron, Aluminum and steel. Besides these, most of the utensils that are used

in the kitchen are made from metals like steel, Aluminum, and Copper (Ngo et al., 2018).

2.3 TYPES OF METAL 3D PRINTING

2.3.1 Powder Bed Fusion

Powder bed fusion (PBF) is a 3D printing process where a thermal energy source selectively melts powder particles (plastic, metal, or ceramic) inside a build area to create a solid object layer by layer. Powder bed fusion 3D printers spread a thin layer of powdered material over the print bed, typically with a type of blade, roller, or wiper. Energy, typically from a laser, fuses specific points on the powder layer, then another powder layer is deposited and fused to the previous layer. The process repeats until the entire object is fabricated. The final item is encased and supported in unfused powder. Although the process varies depending on whether the material is plastic or metal, PBF can create parts with high mechanical properties including strength, wear resistance, and durability for end-use applications in consumer products, machinery, and tooling. Although the 3D printers in this segment are becoming more affordable (starting prices hover around $25000 to $1million), it is considered professional or industrial technology. The materials used in this technology are Plastic powders, metal powders and ceramic powders. And the common applications this technology offers are functional parts, complex or low-run part production (Fu & Körner, 2022)

2.3.1.1 Selective Laser Sintering (SLS)

Figure 2.1 shows Selective laser sintering (SLS) technology that can create objects out of plastic powder by using a laser. First, a bin of polymer powder is heated to a temperature just below the polymer's melting point. Next, a recoating blade or wiper deposits a very thin layer of the powdered material – typically 0.1 mm thick – onto a build platform. A laser (CO2 or fiber) then begins to scan the surface according to the pattern laid out in the digital model.

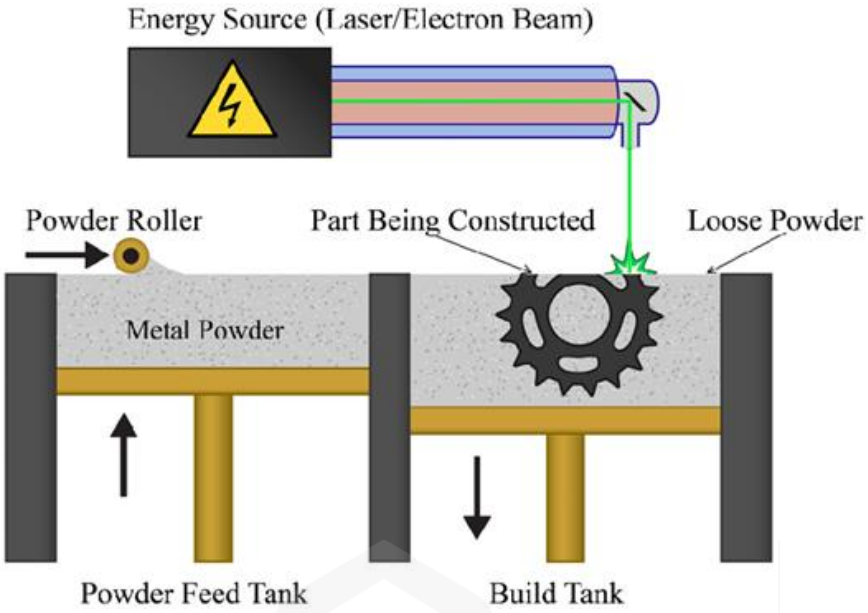

Figure 2.1 Schematic view of SLS method (Jahani et al., 2020)

The laser selectively sinters the powder and solidifies a cross-section of the object. When the entire cross-section is scanned, the build platform moves down one layer thickness in height. The recoating blade deposits a fresh layer of powder on top of the recently scanned layer, and the laser will sinter the next cross-section of the object onto the previously solidified cross-sections. These steps are repeated until all objects are manufactured. The powder that hasn't been sintered remains in place to support the objects, which reduces or eliminates the need for support structures. After removing the part from the powder bed and cleaning, there are no other required post-processing steps. The part can be polished, coated, or colored. There are dozens of differentiating factors among SLS 3D printers, including not only their size but the power and number of lasers, the spot size of the laser, the time and manner in which the bed is heated, and how the powder is distributed, to name just a few. The most common material in SLS 3D printing is nylon (PA6, PA12), but parts can also be printed to be flexible using TPU and other materials (Kinstlinger et al., 2016).

2.3.1.2 Laser Powder Bed Fusion (LPBF)

Figure 2.2 shows a Laser Powder Bed Fusion (LPBF) technology which is a metal 3D printing technique that uses one or more high-powered lasers to melt metal powder layer by layer according to a digital model. It is also known as Direct Metal Laser Sintering (DMLS) or Selective Laser Melting (SLM). LPBF 3D printers have a sealed build chamber filled with inert gas to prevent oxidation and debris. They use a recoater blade or roller to spread the powder on the build plate, where the laser fuses it into the desired shape. The build platform then moves down, and another layer of powder is applied and fused to the previous one. This process repeats until the object is complete. The object is supported by the packed powder and some additional supports. After printing, the object is removed, cleaned, and heat-treated to relieve stresses. The unused powder can be reclaimed and reused. LPBF can produce complex metal parts with high precision and accuracy for various applications in aerospace, medical, and industrial sectors. LPBF machines can use different types of lasers and common engineering alloys, such as stainless steels, nickel superalloys, and titanium alloys (Chowdhury et al., 2022).

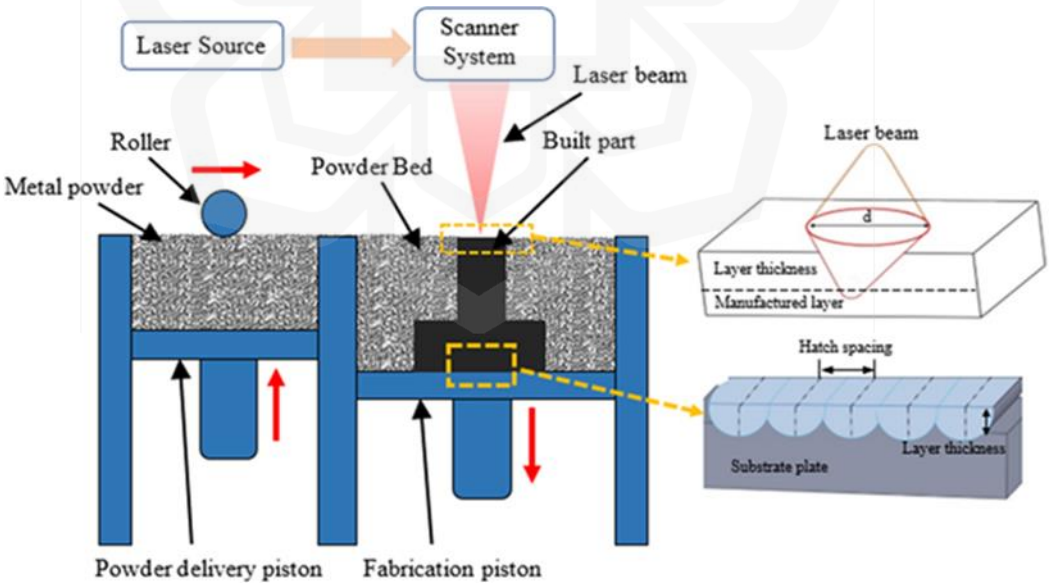

Figure 2.2 Schematic diagram of LPBF or SLM 3D printer (Karabulut & Ünal, 2022)

2.3.1.3 Electron Beam Melting (EBM)

Figure 2.3 shows the schematic diagram of Electron Beam Melting (EBM) or Electron Beam Powder Bed Fusion (EB PBF) technology which is a metal 3D printing technique that uses an electron beam to melt metal powder layer by layer in a vacuum chamber. It can produce parts such as titanium implants, turbine blades, and copper coils. EBM has some advantages over LPBF, which uses a laser instead of an electron beam. EBM can process conductive and reflective metals, generate more power and heat, move faster and expose multiple areas at once, and nest or stack parts without attaching them to the build plate. EBM also has some drawbacks compared to LPBF, such as larger layer thicknesses, lower surface quality, and higher build chamber temperature. EBM printed parts may not require post-print heat treatment to reduce stresses (Tamayo et al., 2021).

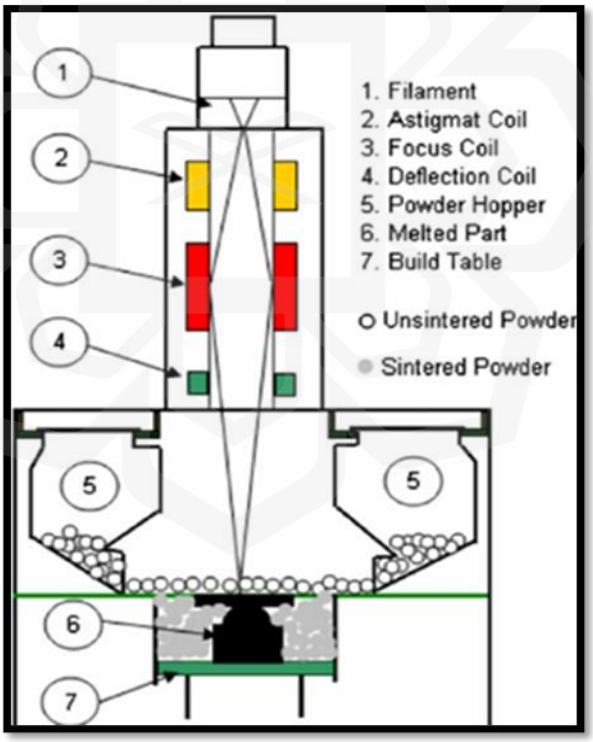

Figure 2.3 Schematic view of EBM method (Syam et al., 2011)

2.4 FDM METAL 3D PRINTING: EVOLUTION AND ADVANCEMENTS

Fused Deposition Modeling (FDM) as shown in Figure 2.4 is a 3D printing technology that was originally developed for plastic printing but has evolved to enable metal printing as well. This technology was first found by S. Scott Crump who cofounded Stratasys. He developed the process in 1988 and received the patent in 1992 (Tim, n.d.) FDM metal 3D printing involves using metal-filled filaments that are extruded through a heated nozzle and deposited layer by layer to form a metal part. FDM metal printing has several advantages, such as low cost, ease of use, and ability to produce complex geometries. It can be used for various applications in aerospace, automotive, and manufacturing industries (Ambrus et al., 2021). In Powder bed fusion technologies such as SLM, SLS, EBM etc. several issues remain unsolved such as high application and machine cost, printing process constraints, and print size restriction.

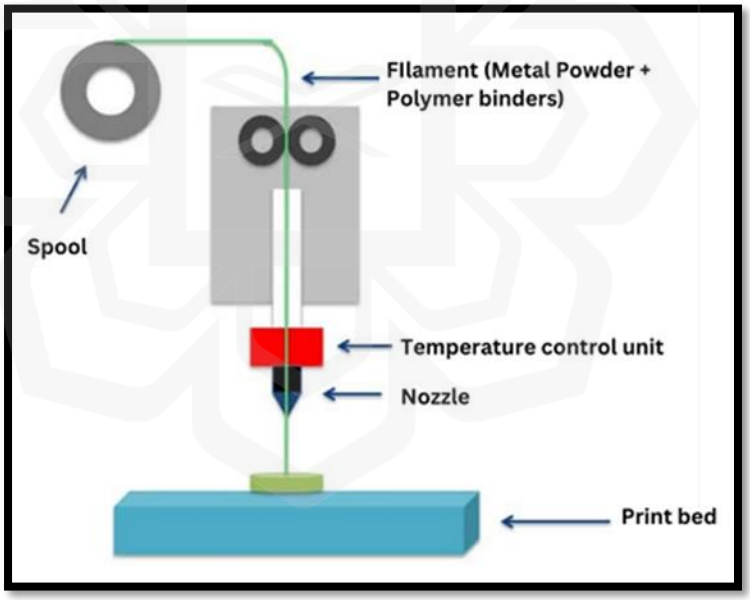

Figure 2.4 Schematic diagram of FDM metal 3D printer

Therefore, Fused deposition modeling technology offers a more affordable alternative for metal 3D printing. However, FDM metal printing also faces some challenges, such as limited material options, post-processing requirements, and low resolution. Previous studies have tried to improve the nozzle design and extruder

designs by implementing techniques like inert gas welding, contact resistance heating, Induction heating to melt metal but these techniques fail to attain the high-resolution parts and also seems to be hazardous to operate.

To overcome these challenges, advancements have been made in various aspects of FDM metal printing such as:

2.4.1 Printer design

New FDM printers have been developed specifically for metal printing, featuring high-temperature extruders, precise control systems, and enclosed build chambers.

2.4.2 Material development

New metal-filled filaments have been introduced, expanding the range of metals that can be printed by FDM, such as titanium, aluminum, copper, and nickel alloys.

2.4.3 Printing accuracy and resolution

Improvements in nozzle and printer design have enabled higher precision and detail in FDM metal prints.

2.4.4 Software and slicing algorithms

Optimization of software and slicing algorithms have ensured better control over printing parameters and toolpaths for FDM metal prints. Most of the current metal 3D printing companies use techniques such as Direct Metal Laser Sintering (DMLS) or Selective Laser Melting (SLM). However, some companies or manufacturers that offer FDM metal 3D printing are described as follows:

Markforged

This company uses a patented process called Atomic Diffusion Additive Manufacturing (ADAM) to print metal parts with a plastic binder that is later removed and sintered (All3DP, 2021).

Virtual Foundry

This company produces a special filament that contains metal powder and a polymer binder. The printed parts can be sintered in a kiln to remove the binder and fuse the metal particles (BRAD WOODS, n.d.).

MakerBot and Ultra fuse

These companies have partnered to offer a similar filament-based metal 3D printing solution that requires debinding and sintering after printing (Gupta, 2023). Our research will use these techniques as a foundation to build upon.

2.5 FILAMENTS USED IN METAL FDM 3D PRINTERS

2.5.1 Metal Filaments for FDM Metal 3D printing

Metal filaments are a type of 3D printing material that contain metal powder and a polymer binder. They can be printed using common FFF 3D printers and then debinded and sintered to obtain pure metal parts with specific properties and applications. The Figure 2.5 shows different types of metal filaments including Copper, Aluminum, Bronze, Titanium, and Ceramic.

Figure 2.5 Images show different types of filaments from Virtual foundry (90% Metal & 10% Polymer)

2.5.2 Metal Filament types and Properties

The types of metal filaments, there composition and melting temperatures are shown in Table 2.1.

Table 2.1 Summarizes the main types and properties of metal filaments (BRAD WOODS, n.d.).

Metal Filament	**Composition**	**Printing Temperature**
Aluminum 6061	65.0-68.5% Al	untested
Bronze	88.0-90.0% bronze	885°C (1625°F)
Copper	87.0-90.0% Cu	1052°C (1925°F)
H13 Tool Steel	86.8% H13 Tool Steel	1260°C (2300°F)
High Carbon Iron	75.0-80.0% Fe	untested
Inconel® 718	82.0-85.0% Inconel® 718	1260°C (2300°F)
Pure Iron	80.0-82.0% Fe	untested
Stainless Steel 17-4	80.0-85.0% Stainless Steel 17-4	1232°C (2250°F)
Stainless Steel 316L	80.0-85.0% Stainless Steel 316L	1260°C (2300°F)

2.6 PROCESS PARAMETERS FOR 3D PRINTING METAL IN FDM 3D PRINTERS

Metal FDM printing involves printing metal filaments with a polymer binder and then debinding and sintering them to obtain pure metal parts. The following are some of the key process parameters for metal FDM printing using the Virtual Foundry copper filament:

So, several studies have been conducted to investigate the effects of these factors on the metal FDM 3D printing process and the properties of the printed metal parts. As (Gordeev et al., 2018) reviewed the recent developments in metal FDM 3D printing technology and discussed the main parameters in each phase of the process. They also explored the application of finite element modelling for metal FDM 3D printing analysis and identified the challenges and gaps in the manufacturing of components. (Ramazani & Kami, 2022b) reviewed the progress on filament materials and process parameters that affect the FDM 3D printing results. They also presented some applications of FDM 3D printing in various fields such as aerospace, automotive, biomedical, electronics, and construction. (Kristiawan et al., 2021) conducted a comprehensive review on FDM based additive manufacturing and covered various aspects such as filament materials, process parameters, post-processing techniques, mechanical properties, applications, and challenges. They also highlighted some future research directions for FDM based additive manufacturing and they also studied the effect of different process parameters on the mechanical properties of Aluminium reinforced ABS thermoplastic composites printed by FDM. They used a commercial FDM printer and optimized the parameters such as layer thickness, infill density, raster angle, and print speed. They found that increasing layer thickness and infill density improved the tensile strength and modulus, while increasing raster angle and print speed reduced them.

Moreover, the mechanical properties of two commercially available Metal-Polymer Hybrid Material filaments which were based on poly lactic acid (PLA), influenced different printing parameters, and measured in elongation and bending tests which concluded that Metal-Polymers blends cannot be used for the rapid manufacturing of objects necessitating mechanical strength (Fafenrot et al., 2017).

Furthermore, a metal 3D printing method was proposed in China by (Dai & Wang, 2019) based on the contact resistance heating theory. The relationships among power, temperature and contact resistance were explored. The heating temperature can reach 800°C and melt the aluminium wire by applying a heat power of approximately 300 W. Similarly, a group of researchers demonstrated that simple design specimens can be successfully fabricated using Metal Inert Gas (MIG) welding in the 3D printing process (Li et al., 2019). Furthermore, Baufeld et al., (2011) had developed a multi-layer single bed wall by combining both laser beam deposition and shaped metal deposition with two different wire-based layer manufacturing techniques. From their result, it is confirmed that these two processes can be used for AM applications. Jandric et al., (2004) had focused on the manufacturing of 3D metal parts using gas tungsten arc welding (GTAW) The result showed that the 3D metal parts have a very uniform microstructure and are free from cracks and porosity. Different from Ghariblu & Rahmati, (2014) who produced layered manufacturing metal parts by combining the additive and subtractive processes. As a result, the part produced had improved geometric accuracy and surface quality of layered parts.

2.7 POST-PROCESSING TECHNIQUES FOR FDM METAL PARTS

After 3D printing metal parts using the Fused Deposition Modeling (FDM) technique, several post-processing techniques can be employed to enhance the final part's properties and aesthetics. Such as by INTEGZA, (2021) a complete post-processing method was carried out where he successfully 3D printed Rocket nozzle using stainless steel composite by two post-processing stages namely Debinding and Sintering. Compared to other techniques such as direct metal laser sintering (DMLS) which uses metal powder for printing, FDM technology is using filament as feedstock material. The composition of the filament is 90% metal and 10% polymer. The idea is that after the3D printing process is done, the post-processing will take place which plays a vital role in metal 3D printing, especially via FDM technology which includes de-binding and sintering. The de-binding process will remove the polymer from the printed parts and finally sintering process turns the remaining material into metal through heating it until the melting point of that specific metal is reached. The study of post-processing (debinding and sintering) temperature, time, porosity and shrinkage effect is very

essential. Selecting the wrong parameters for post-processing will affect the structure of 3D-printed parts. Porosity for example requires optimum control for the management of fracture propagation. Other factors that require consideration during metal additive manufacturing are surface roughness, material flaws and anisotropic behaviors. High surface roughness causes fatigue loading which leads to stress concentrations and early failure. To overcome those limitations here are some common post-processing techniques for FDM metal parts:

2.7.1 Debinding

If a metal filament with a polymer matrix is used, debinding is typically the first step in post-processing. It involves removing the polymer binder from the green part. Debinding can be achieved through various methods such as thermal debinding, solvent debinding, or a combination of both. Solvent de-binding typically happens inside a vapor degreaser using a special de-binding fluid. Depending on the parts, makeup and the binders used, de-binding occurs by either immersing parts in the boiling de-binding fluid, holding it inside the vapor blanket inside the vapor degreaser, or a combination of both. The low-boiling de-binding fluid melts the wax binder. It also creates porosity or channels within the green part that allows the fluid to evaporate quickly before sintering (Ni et al., 2018). A typical de-binding cycle takes 6-20 minutes, but the parts come out dry and cool enough to immediately transfer to the sintering oven. This translates into shorter de-binding cycles and faster production runs overall.

2.7.2 Sintering

Sintering is a crucial step in the post-processing of FDM metal parts. It involves heating the debinded part in a controlled atmosphere to a temperature just below the metal's melting point. During sintering, the metal particles fuse together, resulting in a solid and dense metal part called a green body. The low-density green body is heated in sintering to remove the porosity and densify the material. Sintering occurs below the melting point of the material using naturally occurring solid-state diffusion processes. These diffusion processes bond the individual powder particles together to form a dense

polycrystalline material of high strength. Clay, pottery, and brick have been sintered in this way sintering for thousands of years. Today this process has evolved into many more applications including ceramic/porcelain, glass, and metals. Post-processing is very crucial to determine the success of printed parts. Controlling the right temperature is very important (Clemens et al., 2021)

2.7.3 Surface Finishing

FDM metal parts often undergo surface finishing techniques to improve their appearance and functional properties. This can include processes like polishing, grinding, sanding, or abrasive blasting to achieve the desired surface texture, smoothness, or aesthetic quality Mechninja M., (2021)

2.7.4 Coating and Plating

Metal parts can be coated or plated to enhance their corrosion resistance, improve wear properties, or provide decorative finishes. Common coating techniques include electroplating, chemical plating, or applying protective coatings such as paints or powder coatings (All3DP, 2021)

2.7.5 Post-Processing Support Removal

If the metal part was printed with support structures, removing them after printing is an essential post-processing step. Support structures are typically removed by hand or using tools like pliers, wire cutters, or machining techniques (Manufactur3d (M.), 2023)

2.7.6 Assembly and Joining

Post-processing may also involve joining multiple metal parts together through techniques like welding, brazing, or adhesive bonding to create complex assemblies or larger structures.

2.7.7 Quality Control and Inspection

Post-processing includes quality control steps such as dimensional measurement, non-destructive testing (NDT), or visual inspection to ensure the final part meets the required specifications and quality standards (Post Processing for FDM Printed Parts | Hubs, n.d.)

2.8 MECHANICAL CHARACTERIZATION AND PERFORMANCE EVALUATION IN FDM METAL PRINTING

FDM metal printing is a process that involves printing metal filaments with a polymer binder and then debinding and sintering them to obtain pure metal parts. The mechanical characterization and performance evaluation of FDM metal parts depend on various factors, such as the material composition, the printing parameters, and the post-processing methods (Ramazani & Kami, 2022b), (Hwang et al., 2015), (Rahmatabadi et al., 2021) .

Some of the common methods for mechanical characterization and performance evaluation in FDM metal printing are:

2.8.1 Shrinkage Values

This method measures the dimensional changes that occur during the cooling and solidification of the metal part after printing. It helps in assessing the accuracy and dimensional stability of the printed parts.

2.8.2 Hardness test

This method evaluates the hardness properties of the printed metal parts by testing their resistance to indentation or deformation. It provides information about the material's suitability for specific applications.

2.8.3 Microstructure

This method examines the microscopic structure of the metal part to understand its grain structure, phase distribution, and any potential defects or anomalies. It helps in evaluating the material's integrity, homogeneity, and potential for mechanical performance.

2.8.4 Chemical Composition

This method verifies the material's elemental composition and ensures it meets the required specifications. Techniques such as spectroscopy or elemental analysis can be employed to determine the chemical composition accurately.

2.9 FDM METAL 3D PRINTING APPLICATIONS IN AEROSPACE, MEDICAL AND AUTOMOBILE FIELD

FDM metal 3D printing has emerged as a powerful additive manufacturing technology with diverse applications. In the aerospace sector, major companies like Lockheed Martin, Boeing, and Airbus are incorporating 3D-printed parts into their aircraft. For instance, Lockheed Martin's F16 fighter aircraft received approval for a 3D-printed metal sump pump cover, marking the first qualified 3D-printed engine component in the US Department of Defense (Jeanne Schweder, 2021) The advantages of FDM metal printing extend to other fields as well. In the medical industry, the technology is being used for implants and customized medical devices. Automobile manufacturers are leveraging FDM metal 3D printing for tooling, fixtures, prototyping, end-use parts,

replacement parts, and modifying existing components, among other applications. Scientific studies in biomedical and automation/automobile fields provide further insights. Research published in biomedical journals highlights the use of FDM metal 3D printing for creating patient-specific implants and customized medical devices (Velásquez-García & Kornbluth, 2021). The application of FDM metal printing in the automobile industry has been studied extensively, with research focusing on its potential in tooling, prototyping, and producing end-use parts for functional assemblies (Hao & Lin, 2020).

Furthermore, FDM metal 3D printing finds application in heat exchangers, which play a critical role in industries such as automotive, aerospace, and energy. The technology enables the production of intricate and optimized heat exchanger geometries, enhancing thermal performance (Gao et al., 2015). The versatility of FDM metal 3D printing is also evident in the creation of customized jewelry and accessories, offering designers and jewelers new avenues for intricate and personalized designs (Ngo et al., 2018). Moreover, educational institutions and research facilities utilize FDM metal 3D printing to explore its capabilities, conduct material studies, and develop innovative applications across various fields (Calì et al., 2020)

2.10 CHAPTER SUMMARY

The literature review explores the advancements and challenges in metal 3D printing, specifically focusing on different types of metal 3D printing technologies and the use of metal filaments in Fused Deposition Modeling (FDM) 3D printers. The review discusses various frameworks and methods used in each article, highlighting their strengths and limitations. Additionally, the conceptual contributions of each article and potential themes are summarized. The introduction emphasizes the increasing global interest in the automation industry and the incorporation of 3D printers in various industries to enhance efficiency and customizability. The importance of metals, their characteristics, and wide-ranging applications are also highlighted. The review then delves into different types of metal 3D printing technologies. Powder Bed Fusion (PBF) is discussed as a process where a thermal energy source selectively melts powder particles to create solid objects. Selective Laser Sintering (SLS), Laser Powder Bed

Fusion (LPBF), and Electron Beam Melting (EBM) are explained as subtypes of PBF, each with its own strengths and limitations.

FDM metal 3D printing, which initially evolved from plastic printing, is explored as a more affordable alternative. The challenges faced by FDM metal printing, such as limited material options and low resolution, are discussed. Advancements in printer design, material development, printing accuracy and resolution, as well as software and slicing algorithms, are highlighted as solutions to overcome these challenges. Several companies offering FDM metal 3D printing solutions are mentioned, including Mark forged, Virtual Foundry, MakerBot, and Ultra fuse. The use of metal filaments in FDM printing is explained, with details provided about the composition, printing temperature, and properties of different types of metal filaments.

The review also covers the process parameters involved in metal FDM printing using copper filaments from Virtual Foundry. It cites previous studies that have investigated the effects of these parameters on the printing process and the properties of printed metal parts. Overall, the reviewed articles contribute to the understanding of different metal 3D printing technologies, advancements in FDM metal printing, and the effects of process parameters on printed metal parts. The potential themes that emerge from the review include the need for affordable metal 3D printing solutions, advancements in printer design and materials, and the optimization of process parameters for improved print quality and mechanical properties.

CHAPTER THREE

RESEARCH METHODOLOGY

3.1 INTRODUCTION

In this chapter, we present the methodology used to investigate the factors influencing the post-processing effects of copper polymer composites fabricated on an FDM 3D printer. The research design and approach, along with the materials and equipment employed, will be discussed in detail. The sample preparation process involves modeling the samples using Computer-Aided Design and configuring the printing parameters to ensure accurate fabrication. The printing process plays a crucial role in determining the quality of the final product. We explored various aspects, including layer height, print speed, nozzle temperature, bed temperature, and infill density, to optimize the printing parameters for the copper polymer composites.

Following the printing stage, post-processing techniques such as debinding and sintering was applied to enhance the properties of the samples. Debinding involves the removal of binders, while sintering facilitates the consolidation of the copper particles. These steps significantly impact the final quality of the composite material. To assess the mechanical properties of the sintered samples, measurements of shrinkage value using micrometers and Vickers hardness testing was performed. Additionally, we analyzed the microstructure and chemical composition of the samples using scanning electron microscopy (SEM) and energy-dispersive X-ray spectroscopy (EDX) analysis, respectively. Throughout the research, data collection and analysis methods were employed to ensure accurate and reliable results. This chapter provides a comprehensive overview of the methodology employed to investigate the post-processing parameters of copper polymer composites using an FDM 3D printer. Figure 3.1 summarizes the representation of the overall research, investigating the post-processing parameters of copper polymer composites using an FDM 3D printer.

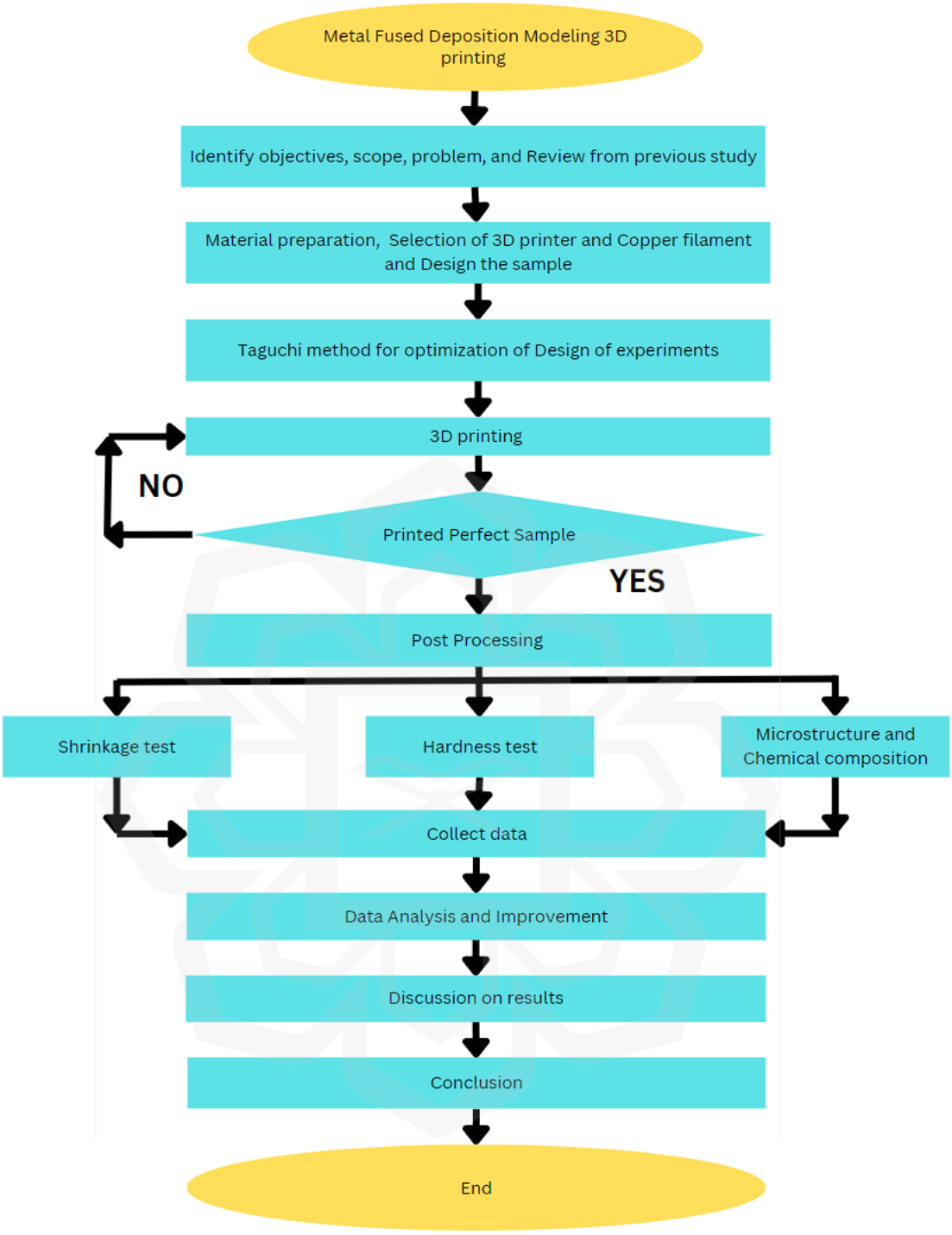

Figure 3.1 Flow chart of overall research

3.2 DESIGN OF EXPERIMENTS

Design of experiments (DOE) is a formal and systematic manner to solve engineering problems that use various principles and techniques to ensure the availability of cogent, sound and supportable results. Fundamental principles are Randomization, Replication, Blocking, Orthogonality and Factorial Experimentation. This change in the independent variables is generally hypothesized. The main aim is to get optimized results in the minimum amount of data. But this method requires intense efforts and valuable time. Processes are controlled by various factors. Similarly, the quality and the purity of a copper composite filament depends on printing parameters like layer height and Infill density and Operating parameters like debinding and sintering which can also affect the purity of 3D printed copper metal part.

3.2.1 Taguchi method for optimization

The Taguchi method is a valuable approach for optimizing results in a minimal number of trials, especially when dealing with a large number of parameters. It utilizes mathematical models to save time and increase effectiveness in the experimental procedure. According to Taguchi, it is essential for the output (Y) to not only stay within specifications but also be centered around the target value. Deviations from the target incur losses, even if within specifications, and larger deviations lead to greater losses. This method considers both conventional design of experiments (DOE) factors and noise factors to build a sustainable model with reduced response variance. Orthogonal arrays are employed in Taguchi's approach, which depend on the degrees of freedom for effective experimentation and analysis.

The objective of this study was to optimize the debinding and sintering holding time and temperature for 3D printed copper-polymer composite samples using the Taguchi method for the design of experiments. The experiment consisted of eight samples, with four samples printed with a layer thickness of 0.3mm and the remaining four samples printed with a layer thickness of 0.4mm. The post-processing steps involved debinding and sintering of the samples.

Table 3.1 L_8 Orthogonal test array layout

Samples	Holding time (hours) (Debinding)	Holding time (hours) (Sintering)	Layer Thickness (mm)
A	2	3	0.3
B	2	3	0.4
C	2	5	0.3
D	2	5	0.4
E	4	3	0.3
F	4	3	0.4
G	4	5	0.3
H	4	5	0.4

To determine the optimized parameters for the experiment, an L8 orthogonal test array was constructed based on the factors and levels mentioned above. Table 3.1 represents the layout of this test array, with each row indicating a specific combination of debinding holding time, sintering holding time, and layer thickness. The samples were labelled as A, B, C, D, E, F, G, and H to denote the different combinations of levels for debinding holding time, sintering holding time, and layer thickness. The experiments were conducted using Table 3.1 as the experimental design, enabling the assessment of the effects of different parameter combinations on the properties and characteristics of the 3D printed copper-polymer composite samples. This methodology allowed for the determination of optimized debinding and sintering holding times that would enhance the final quality of the samples.

The factors considered in this experiment were the holding time for debinding, holding time for sintering, and layer height. Two levels were selected for each factor as shown in Table 3.2. For the debinding process, Level 1 involved a two-step temperature ramping procedure. The samples were held at 240°C for 30 minutes and then at 480°C for 4 hours. In Level 2, the debinding process consisted of four temperature steps: 120°C, 240°C, 360°C (each for 30 minutes), and finally 480°C for 4 hours.

Regarding the sintering process, Level 1 encompassed three temperature steps. The samples were held at 350°C for 30 minutes, followed by 700°C for 30 minutes, and finally reaching 1050°C, where they were held for 5 hours. In Level 2, the sintering process included five temperature steps: 250°C, 480°C, 720°C, and 960°C (each for 30 minutes), and then 1050°C for 5 hours.

Table 3.2 L8 Orthogonal array 3 parameters checked at 2 Levels

Parameters	Holding Time (hours) (Debinding)	Holding Time (hours) (Sintering)	Layer height (mm)
Level 1	2	3	0.3
Level 2	4	5	0.4

3.3 MATERIALS AND EQUIPMENT

3.3.1 Selection of Copper composite Filament

Figure 3.2 Sample of Copper Polymer Composite Filament used for the experiment

The metal filament used was a copper polymer composite, consisting of 90% copper powder and 10% polymer material. This filament was sourced from the company called the Virtual Foundry, which is based in the United States. The copper polymer composite filament provided the necessary properties required for 3D printing metal components using the FDM (Fused Deposition Modeling) technology. Its composition of 90% copper powder ensured a high concentration of the metal, enabling the subsequent conversion into pure copper during the post-processing steps. The 10% polymer material acted as a binder and facilitated the printing process by providing stability and compatibility with the 3D printer. Copper is a soft, ductile metal used primarily for its electrical and thermal conductivity. Copper's high conductivity makes it an ideal material for many heat sinks and heat exchangers, power distribution components such as bus bars, manufacturing equipment including spot welding shanks, antennae for RF communications, and more. The ability to print pure copper using Metal FDM 3D printer enables geometrically optimized parts that were previously expensive, time consuming, or impossible to make.

Figure 3.3 Properties of Copper-Polymer Composite Filament (BRAD WOODS, n.d.)

General information	
Manufacturer	The Virtual Foundry (USA)
Material	Copper (89 %) + PLA
Format	Spool of 500 g
Density	4.5 g/cm3
Amount of metal (volume)	66 %
Amount of metal (mass)	89 %
Diameter of filament	1.75 or 2.85 mm
Filament length	±47 m (Ø 1.75 mm - 0.5 kg)
	±17 m (Ø 2.85 mm - 0.5 kg)
Color	Reddish

3.3.2 Selection of FDM 3D printer

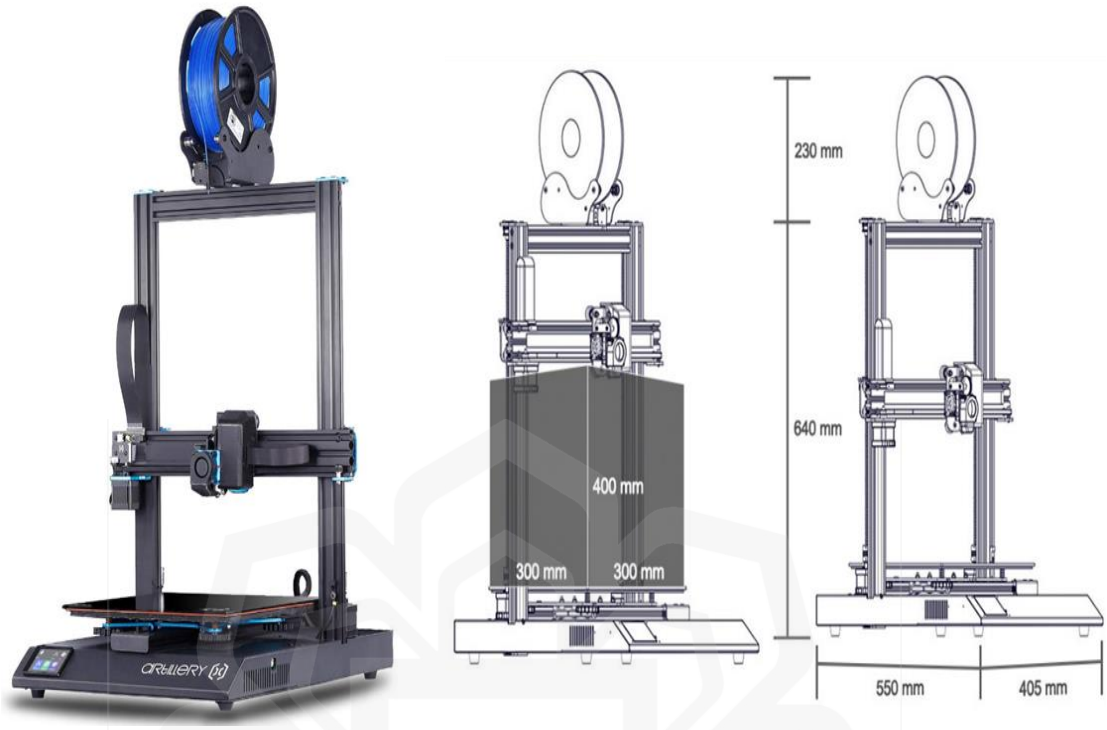

Figure 3.4 A typical low cost FDM 3D Printer (*Artillery Sidewinder X*, n.d.)

The specific equipment utilized in the study was the Artillery (Evnovo)® Sidewinder X1 3D Printer, a low-cost direct extruder Fused Deposition Modeling (FDM) 3D printer. This model of 3D printer was chosen for its affordability and compatibility with the research objectives. The Artillery Sidewinder X1 3D Printer typically costs around RM 2000. The Artillery Sidewinder X1 3D Printer features a direct extruder setup, where the filament is fed directly into the extruder assembly. This design allows for more precise filament control and facilitates the printing of copper polymer composite materials. Additionally, the Artillery Sidewinder X1 3D Printer includes a touchscreen interface for intuitive operation and control of the printing process. It supports a range of filament materials and offers a sizable build volume, enabling the production of larger or more complex parts. By utilizing the Artillery Sidewinder X1 3D Printer, the study aimed to investigate the feasibility and performance of printing copper polymer composite materials and subsequent conversion into pure metal using a cost-effective and easily accessible 3D printing system.

Table 3.3 Specifications of FDM 3D printer (*Artillery Sidewinder X*, n.d.)

Layer Resolution	0.1mm
XYZ Positioning Accuracy	0.05mm, 0.05mm, 0.1mm
Printing Filament	Metal Polymer composite, PLA, ABS, TPU, Flexible Materials,
Nozzle Diameter	0.4mm, 0.6mm, 0.8mm, 1mm
Machine Dimensions	550 x 405 x 640 mm
	550 x 405 x 870 mm (width spool holder)
Maximum Print Speed	150mm/s
Build Volume	300 x 300 x 400 mm
Extrude Type	Titan Extruder (Direct Drive)
Maximum Build Plate Temperature	130°C
Power Requirement	110V/220V
	650 W max

3.4 SAMPLE PREPARATION

3.4.1 Sample modelling in Computer Aided Design

For this research, Blender modeling software, was employed to design the samples. The dimensions of each sample were set to length 25mm, width 25mm and height 5mm, ensuring consistency and uniformity throughout the experiment. To maximize productivity and resource utilization, eight samples were designed together in a single CAD file, eliminating the need for repeated printing as shown in Figure 3.4.

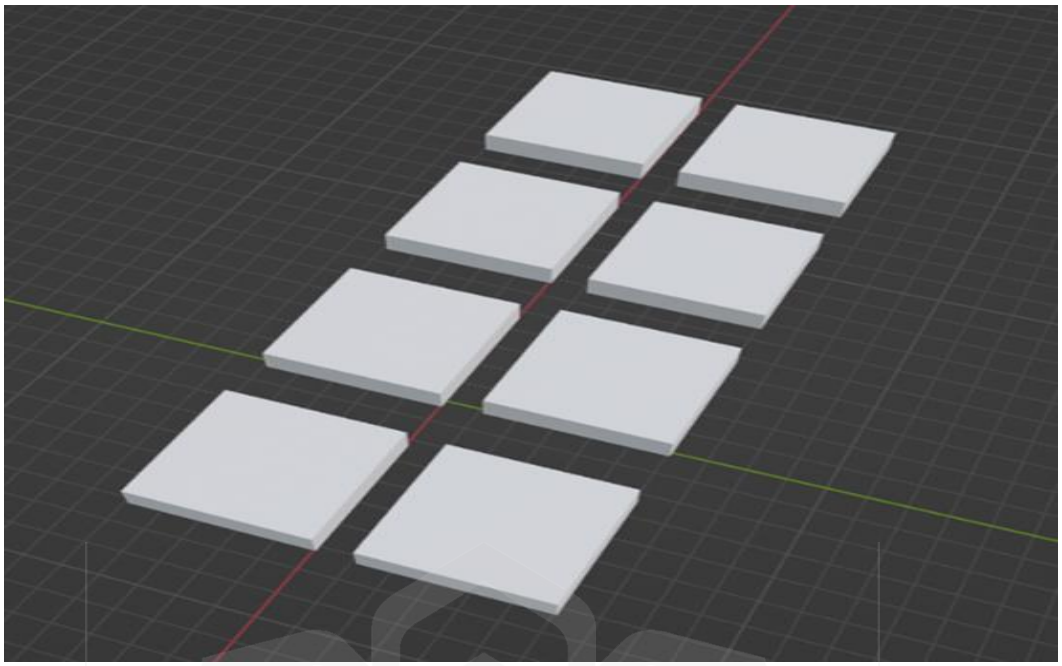

Figure 3.5 Image illustrating 8 samples designed in CAD software

This approach not only reduced material waste but also minimized the time required for sample fabrication. By leveraging the capabilities of Solid Edge, the researcher could precisely model and visualize each sample, ensuring accurate representation before the physical production stage. The ability to create multiple samples simultaneously within the software streamlined the entire sample preparation process, contributing to improved efficiency and reliability in subsequent testing and analysis.

3.4.2 Setting up the Printing parameters

3.4.2.1 Printing Parameters

In this section, we will outline the printing parameters employed for two sets of samples, aimed at investigating the influence of layer thickness on post-processing outcomes. The first set consisted of eight samples printed with a layer height of 0.3mm, while the second set comprised eight samples printed with a layer height of 0.4mm. The analysis

of post-processing results will provide valuable insights into the sintering behaviour and the quality of the printed metal components.

3.4.2.2 Spool Placement

In order to reduce pull and friction, careful consideration was given to the placement of the spool. However, for Bowden-fed printers, it was necessary to place the spool next to or under the feeder to ensure a smooth filament feed. It should be noted that the filament used in this study, consisting of 90% Copper metal powder and 10% thermoplastic binder, which is particularly fragile, resulting in low filament strength. Even a slight pull or bending can cause the filament to break, making it unsuitable for Bowden-fed 3D printers.

3.4.2.3 Nozzle Selection

A nozzle with a diameter of 0.6mm made of hardened steel, was utilized for printing with the Copper composite Filament. The nozzle temperature was initially set at 210°C (410°F) and adjusted within the range of 190-230°C (374/446°F) to optimize printing conditions. Fine-tuning the nozzle temperature allowed for better control over the printing process and ensured appropriate filament behavior.

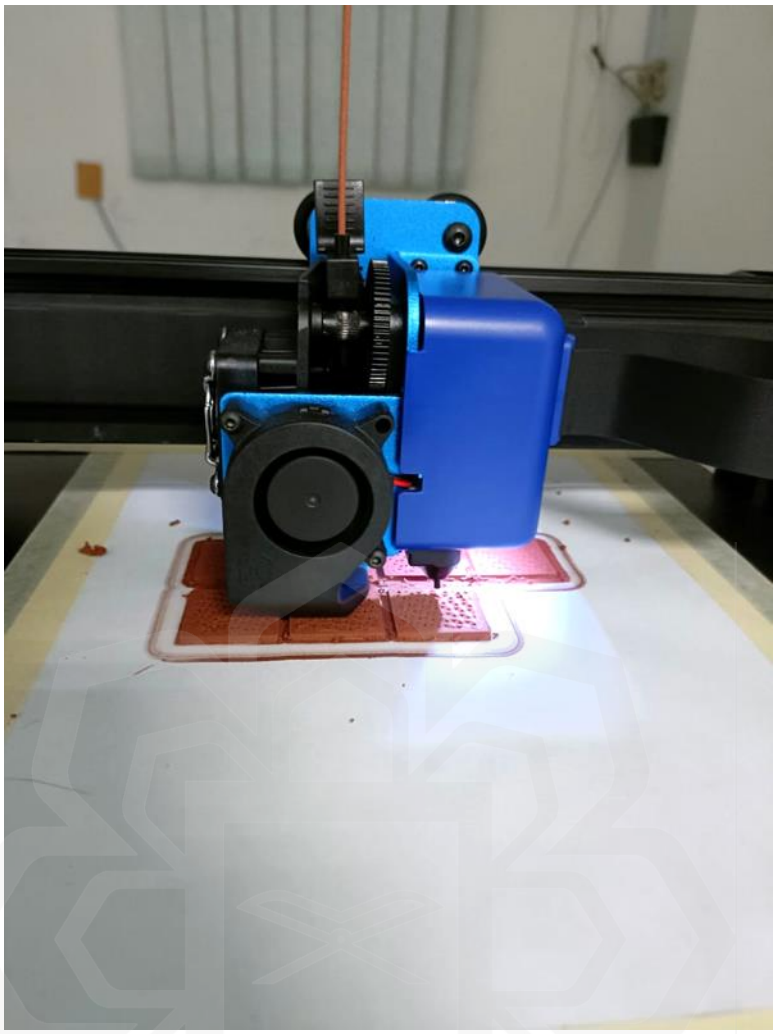

Figure 3.6 Shows the samples printed on a piece of white paper

The approach to preparing the build plate varied depending on the material used. The specific guidelines implemented in this study involved avoiding direct printing onto the Glass Build Plate due to the risk of prints welding onto it. Instead, to facilitate easy removal of prints and the printed samples, a sheet of paper was securely taped onto the build plate using paper tape. Additionally, as an optional step to enhance overall print quality, the print bed temperature was set to a range of 70°C-80°C, ensuring that the paper used for easy removal was not affected by this temperature. Alternatively, a flexible and heat-resistant silicon plate could be employed as an alternative to the paper for covering the print bed.

3.4.3 Printing Parameters for the First Set of Samples (Layer Height: 0.3mm)

3.4.3.1 Layer Height

The layer height defines the thickness of each printed layer. In this set, a layer height of 0.3 mm was chosen as the baseline parameter to examine its impact on the post-processing results.

3.4.3.2 Top Layers

Five top layers were added to ensure sufficient surface quality and strength in the printed samples.

3.4.3.3 Top and Bottom Thickness

A uniform top and bottom thickness of 1.75mm was set to maintain structural integrity.

3.4.3.4 Bottom Layers

Five bottom layers were included to provide a solid foundation for the samples during printing and post-processing.

3.4.3.5 Infill Density

To optimize material consumption and part durability, an infill density of 80% was chosen as shown in Figure 3.6. Moreover, infill density was a significant factor as it did not affect the shrinkage value significantly.

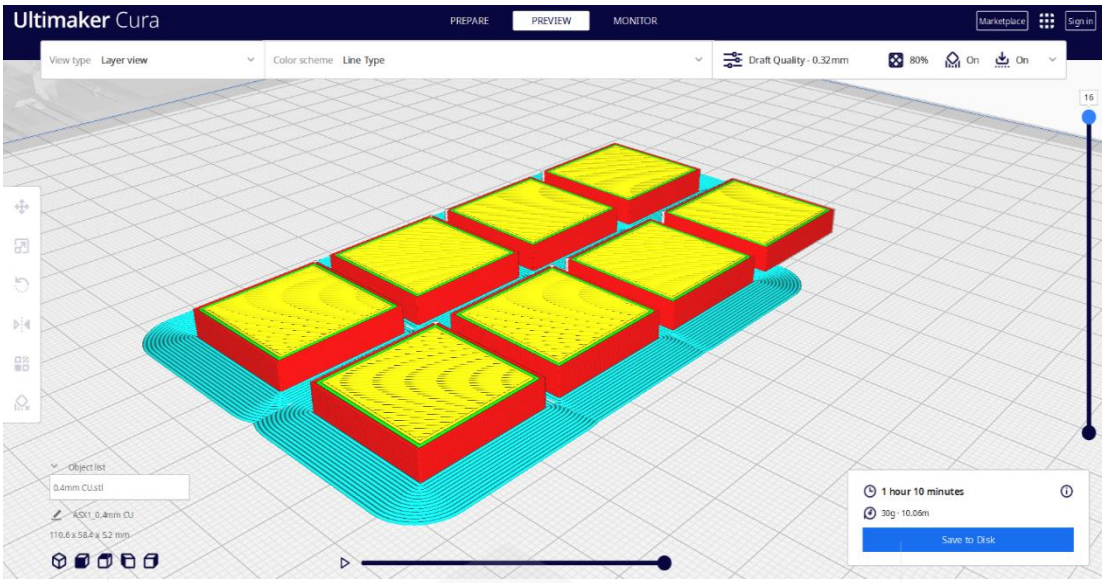

Figure 3.7 Displays the samples infill density

3.4.3.6 Infill Patterns

As shown in Figure 3.7, the infill pattern was chosen as triangles, which is a common pattern that offers a good trade-off between strength and material use. Other patterns such as line, honeycomb, cubic, etc., were not suitable for printing metal composite filament, as the material tended to detach from the part instead of sticking to it. Therefore, the triangular pattern was the strongest and the cleanest infill pattern for this type of filament.

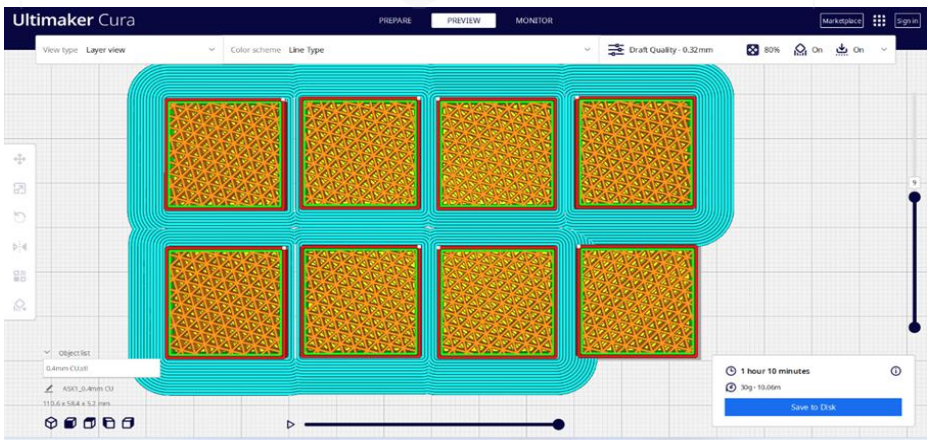

Figure 3.8 Illustrates the triangular infill pattern for the sample

3.4.3.7 Printing Temperature

The printing temperature was maintained at 200 degrees Celsius to ensure proper fusion and layer adhesion.

3.4.3.8 Build Plate Temperature and Adhesion

The build plate was heated to 80 degrees Celsius to enhance adhesion between the print and the build surface. Paper tape was used to secure the paper onto the printing bed, acting as an adhesion layer for the samples.

3.4.3.9 Print Speed

The printing speed was set to 60 mm/s, ensuring a balance between print quality and production time.

3.4.3.10 Fan Speed

The fan speed was set to 100 to facilitate cooling and prevent warping during printing.

3.4.4 Printing Parameters for the Second Set of Samples (Layer Height: 0.4mm)

3.4.4.1 Layer Height

The layer height for this set of samples was increased to 0.4mm to investigate the impact of thicker layers on the post-processing results.

3.4.4.2 Remaining Parameters

All other printing parameters, including the number of top layers, top and bottom thickness, bottom layers, infill density, infill pattern, printing temperature, build plate temperature and adhesion, print speed, and fan speed, remained the same as in the first set of samples.

The variation in layer thickness between the two sets of samples allows us to evaluate the influence of this parameter on the post-processing steps, such as debinding and sintering. By comparing the results of the two sets, we can assess the impact of layer thickness on the dimensional accuracy, distortion, and quality of the sintered metal components.

Table 3.4 Printing Parameters for the first and second set of samples

Printing Parameters	**Values**
Layer Height	0.3 mm for First set of samples, and 0.4 mm for second set of samples.
Top Layers	Five Layers
Top and Bottom Thickness	1.75mm
Bottom Layers	Five Layers
Infill Density	80%
Infill Pattern	Triangular Pattern
Printing Temperature	200 degrees Celsius
Build Plate Temperature and Adhesion	80 degrees Celsius
Print Speed	60 mm/s
Fan Speed	100 rpm

3.5 POST PROCESSING

In this subsection, we outline the post-processing steps involved in the debinding, and sintering of the copper composite 3D printed samples. For debinding and sintering process the apparatus used are shown in Figure.3.8

Figure 3.9 Images of the apparatus used in post processing: (A) Aluminum Oxide (Al2 O3), (B) Debinding and Sintering Furnace (C) Talcum Powder for Sintering (D) Sintering Carbon (E) Ceramic Crucible (F) Porcelain lid for crucible to conserve the sintering carbon

3.5.1 Debinding

Debinding is a crucial step in the post-processing of metal 3D printed samples. The debinding process removes the binder material from the green parts before sintering.

For the debinding process, two different furnaces were used due to variations in the samples.

In the debinding phase of the operation, the plastic that holds the filament and then the print together is removed through a Thermal Debinding Process. The Virtual Foundry's thermoplastic which is only 10% in the filament material is designed to be cleanly removed from the printed part at temperatures between 427°C/800°F and 482°C/900°F. It's important to ramp the temperature slowly up to this point in order to avoid distortion of the samples. For example, heating too quickly will cause the plastic to boil before it's removed from the part. This boiling action will create voids in the final sintered part.

The debinding steps are as follows:

1. Firstly, the researcher needs to bury the part in Aluminum oxide (AL_2-O_3).
   a. Then the crucible must be filled with an initial layer of (AL_2-O_3).
   b. Then the green part must be placed on the initial bed as shown in Figure 3.9(A).
   c. Then the part should be covered with more (AL_2-O_3).
2. It's important that at least ½" or 15mm of (AL_2-O_3) must be on top of the part and the researcher should make sure that every corner is filled properly in the crucible by adding (AL_2-O_3) and slowly tapping the edge of the Crucible so the (AL_2-O_3) settles into place.
3. Place Crucible into the furnace as shown in the Figure 3.9(B). After placing the crucible, the researcher needs to program the Furnace to ramp to 480°C and hold it up to 4 hours. Following is the design of experiments obtained from Taguchi method for Debinding 8 samples.

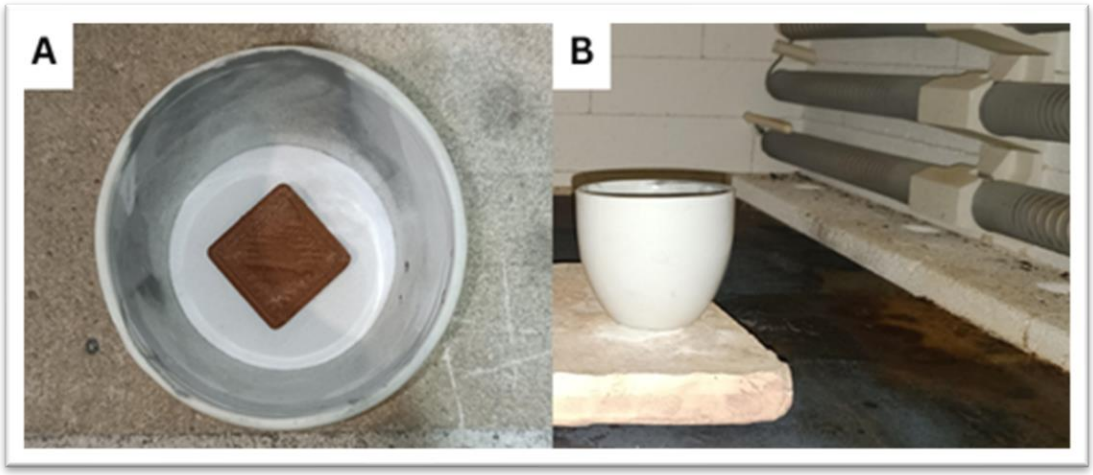

Figure 3.10 The above images show the Crucible preparation for Debinding, (A). The sample is kept on the Aluminum Oxide and top of the sample was further covered with Aluminum oxide layer up to ½" or 15mm, (B). The Crucible is placed into the Furnace

3.5.1.1 Debinding Samples A, E, B, F in (FURNACE 1)

- Start by placing the samples in the furnace at a temperature of 120°C and hold for 30 minutes.
- Ramp up the temperature to 240°C and hold for 30 minutes.
- Increase the temperature again to 360°C and hold for 30 minutes.
- Finally, ramp up the temperature to 480°C and hold for 4 hours.
- Allow the furnace to cool,

3.5.1.2 Debinding Samples C, D, G, H in (FURNACE 2)

- Begin by placing the samples in the furnace at a temperature of 240°C and hold for 30 minutes.
- Ramp up the temperature directly to 480°C and hold for 4 hours.
- Allow the furnace to cool down to room temperature.
- Then the crucible must be emptied and the sample must be removed which completes the debinding process

At this phase, the part will be strong enough to handle, but is still quite fragile. So, need to be carefully handled. The part at this phase is called a "brown" part.

3.5.2 Sintering

After the debinding process, the samples were sintered to achieve the desired final properties. Different sintering temperatures were employed for the two sets of samples.

The Sintering steps are as follows:

1. Firstly, the crucible must be filled halfway with Talcum powder Figure.3.10(B).
2. Then gently the part should be placed on top of this first layer of Talcum powder and then the part must be buried at least ½" or 15mm from the top and some space should be left from the top of the crucible to add a layer of Sintering Carbon, as in Figure 3.10(C, D, E)
3. The carbon becomes chemically active at higher temperatures and will combine with any oxygen, creating an oxygen free atmosphere.
4. And now Sintering Carbon must be added up to ½" or 15mm layer, then the lid must be kept on top of the crucible as in Figure 3.10(F, G, H)
5. The crucible must be placed in the Furnace as shown in Figure 3.10(I) and now the researcher must program the Furnace to slowly ramp to a temperature of 1050°C and hold it up to 5 hours. Following is the design of experiments obtained from Taguchi method for Sintering the 8 samples.

3.5.2.1 Sintering Samples A, E, B, F in (FURNACE 1)

- Start the sintering process at a temperature of 210°C and hold for 30 minutes.
- Ramp up the temperature to 420°C and hold for 30 minutes.
- Increase the temperature to 630°C and hold for 30 minutes.
- Further ramp up the temperature to 840°C and hold for 30 minutes.

- Finally, ramp up the temperature to 1050°C and hold for 5 hours.
- Allow the furnace to cool down to room temperature.

3.5.2.2 Sintering Samples C, G, D, H in (FURNACE 2)

- Begin the sintering process at a temperature of 3 50°C and hold for 30 minutes.
- Ramp up the temperature to 700°C and hold for 30 minutes.
- Finally, ramp up the temperature to 1050°C and hold for 5 hours.
- Allow the furnace to cool down to room temperature.
- Then the crucible must be emptied and the sample must be removed and brushed off for removing any remaining carbon which completes the Sintering process.

After the sintering process the samples should be worked with a wire brush or wheel and these samples must undergo sanding process with various grit sizes which can result to shiny metal part.

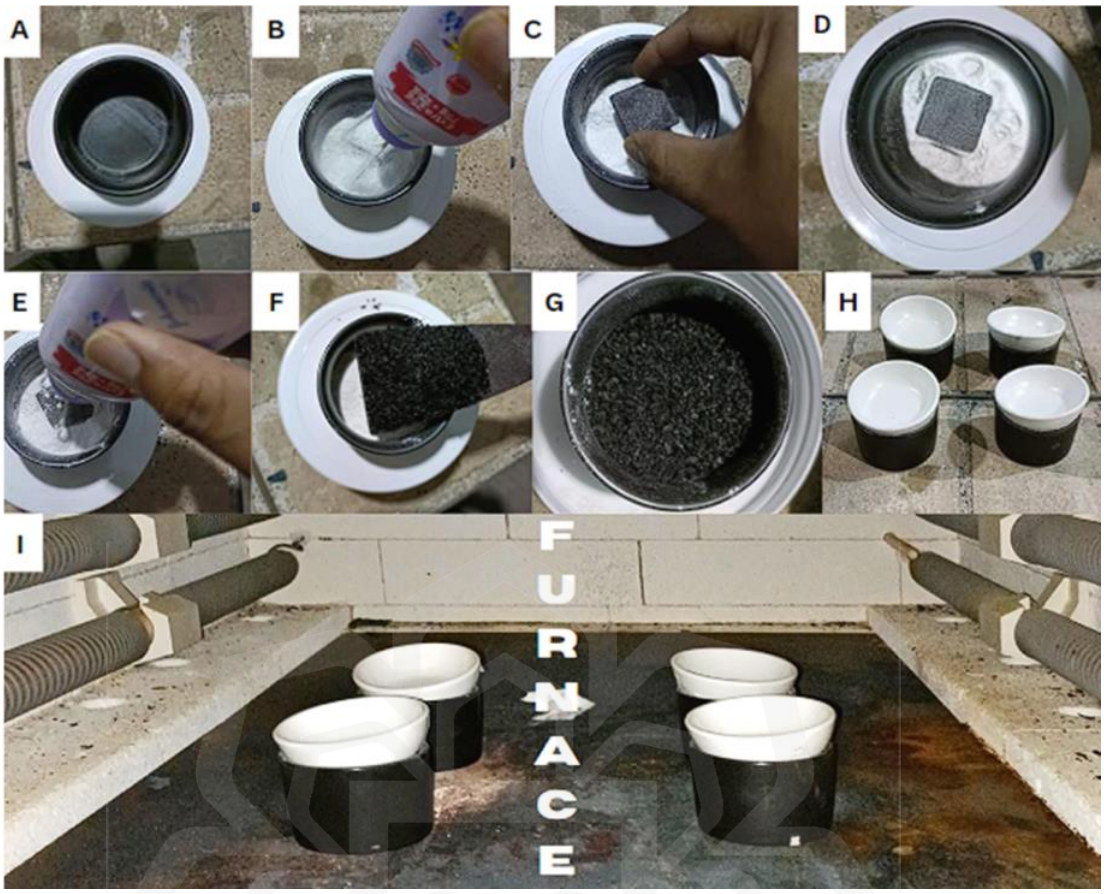

Figure 3.11 The above images show the Crucible preparation for Sintering, (A). An empty crucible, (B). Putting the first layer of Talcum Powder, (C). Placing the debinded sample on the first layer of Talcum Powder, (D). Illustrates the sample position, (E). The sample is covered with talcum, (F). Putting the Sintering Carbon on the talcum powder, (G). Crucible covered with the Sintering Carbon, (H). White Porcelain Lid covering the crucible to sustain the Sintering Carbon. (I). Samples kept in the Furnace for Sintering

3.6 MECHANICAL PROPERTIES

In this section, we describe the methodology for conducting mechanical analysis on the samples after the debinding and sintering processes. The mechanical properties include the measurement of shrinkage values using micrometers, Vernier calipers, and a weight machine, as well as Vickers hardness testing for sintered copper polymer samples.

3.6.1 Measurement of shrinkage value

To determine the shrinkage values of the samples, the following equipment and tools were used

3.6.1.1 Micrometre

Figure 3.12 The above image shows the micrometer for measuring the values in z-axis

Measurements should be taken using a micrometer as shown in Figure.3.11, which is a precision instrument that is capable of measuring small distances accurately. The micrometer allows for precise measurements of the dimensional changes in the samples after the debinding and sintering processes.

3.6.1.2 Vernier Calliper

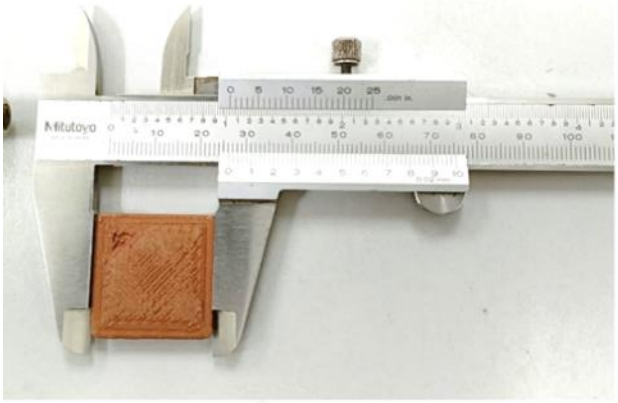

Figure 3.13 The above image shows the Vernier caliper used for measuring the sample values in x and y axis

Vernier caliper was employed to measure the dimensions of the samples, including length in X axis, width in Y axis, and height in Z axis. This instrument provides accurate and reliable measurements, facilitating the determination of shrinkage values.

3.6.1.3 Weight Machine

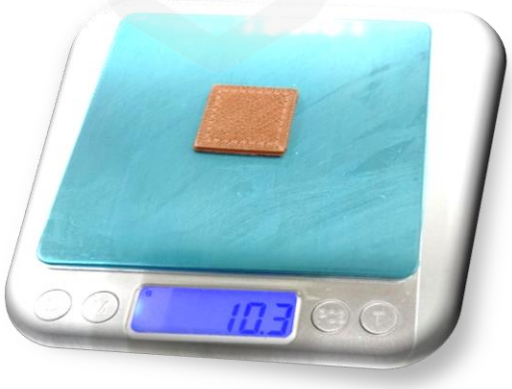

Figure 3.14 A mini electronic precision scale used for measuring the weight of the samples in grams

A mini electronic precision scale was used as shown in Figure.3.13, to measure the weight of the samples before and after the debinding and sintering processes. The weight difference can provide additional insights into the overall shrinkage of the samples.

3.6.2 Vickers Hardness test

The hardness of the samples was tested using the FALCON 600 hardness tester as shown in Figure 3.14, a device by INNOVATEST Europe BV. The Vickers hardness test was performed with the following parameters:

Figure 3.15 Vickers Hardness Tester Falcon 600

Hardness Scale HV-2 Dwell Time: 10 seconds, The steps for the Vickers hardness test were as follows:

The Vickers hardness scale (HV) was selected, with a maximum of 2kg, to measure the hardness of the samples. This scale uses a diamond pyramid indenter to measure the material's resistance to indentation.

The Vickers hardness number (HV) was calculated by measuring the diagonals of the indentation left by the indenter. This number indicated the hardness of the samples, reflecting their ability to withstand external forces. The test was repeated five times on different locations of the sample, and the results were recorded in a table.

3.7 MICROSTRUCTURE AND CHEMICAL ANALYSIS

Figure 3.16 The above images show the Scanning Electron Microscope used for analyzing the microstructure of the samples

In this subsection, we describe the methods used for the microstructure analysis and chemical composition determination of the 3D printed samples. Two techniques, Scanning Electron Microscopy (SEM) and Energy-Dispersive X-ray Spectroscopy (EDX), were employed for these analyses.

Scanning Electron microscopy for microstructure analysis:

Microstructure analysis provides valuable insights into the internal structure and surface morphology of the sintered copper composite samples. Scanning Electron Microscopy (SEM) was employed to examine the microstructural features at high magnification, utilizing specific parameters for analysis. SEM analysis was conducted for all eight samples using a high-resolution scanning electron microscope equipped with secondary electron imaging mode as shown in Figure 3.15.

To investigate the microstructural characteristics, the samples were carefully sectioned to expose their internal structure. Subsequently, a thin conductive layer was applied to the prepared samples, enhancing electron conductivity and minimizing charging effects during imaging by using the Plasma arc coating machine as shown in Figure 3.16

Figure 3.17 The above image shows the Sputter coater used for coating the samples before SEM analysis

The SEM analysis was performed by varying the parameters of accelerating voltages and beam currents. Different combinations of parameters, including SED 10.0 KV to SED 20.0 kV and WD 10mm to WD 20mm, were utilized to capture detailed images of the samples. Additionally, the microscope was set to HV x100 to x500

magnification to explore the samples at varying levels of detail, ranging from 50 micrometers to 100 micrometers. By employing these specific parameters, the SEM analysis enabled the examination of surface topography, grain morphology, and the identification of any potential defects present within the sintered copper composite samples.

3.7.1 Energy-dispersive X-ray spectroscopy (EDX) analysis for chemical composition

To determine the elemental composition of the samples, Energy-Dispersive X-ray Spectroscopy (EDX) analysis was employed. EDX is a non-destructive technique that provides qualitative and quantitative information about the chemical elements present in the sample. EDX analysis was conducted for all eight samples to obtain insights into their chemical composition. The SEM instrument used for microstructure analysis was equipped with an EDX detector. During the analysis, the electron beam interacted with the sample, resulting in the emission of characteristic X-rays from the elements present. The emitted X-rays were detected and analyzed to determine the elemental composition of the samples. The collected data were processed using specialized software, which allowed for the identification and quantification of the elements present in the samples. By combining the information obtained from SEM microstructure analysis and EDX chemical composition analysis, a comprehensive understanding of the internal structure and elemental composition of the printed samples was achieved. These analyses played a vital role in evaluating the quality and integrity of the printed samples, as well as providing insights into the effects of different printing parameters on the resulting microstructure and chemical composition.

3.8 CHAPTER SUMMARY

Chapter 3 provides an in-depth overview of the research methodology employed to investigate the factors influencing the post-processing effects of copper polymer composites fabricated on an FDM 3D printer. The chapter begins with an introduction to the research design and approach, emphasizing the importance of printing parameters

and post-processing techniques in determining the final quality of the composite material. The chapter highlights the significance of the printing process and explores various aspects such as layer height, print speed, nozzle temperature, bed temperature, and infill density. These parameters are optimized to ensure accurate fabrication of the copper polymer composites. Post-processing techniques, including debinding and sintering, are then discussed, as they significantly impact the properties of the samples. Debinding involves the removal of binders, while sintering facilitates the consolidation of the copper particles. To assess the mechanical properties of the sintered samples, measurements of shrinkage value and Vickers hardness testing are performed. Additionally, the microstructure and chemical composition of the samples are analyzed using scanning electron microscopy (SEM) and energy-dispersive X-ray spectroscopy (EDX) analysis, respectively. The chapter emphasizes the use of data collection and analysis methods to ensure accurate and reliable results throughout the research. It concludes by summarizing the research design and providing a flow chart representation of the overall investigation.

Furthermore, the chapter introduces the Taguchi method as a valuable approach for optimizing the debinding and sintering holding times for the 3D printed copper-polymer composite samples. An L8 orthogonal test array is constructed to determine the optimized parameters, and the effects of different parameter combinations on the properties and characteristics of the samples are assessed. The materials and equipment used in the study are also described. The copper polymer composite filament, consisting of 90% copper powder and 10% polymer material, is selected for its suitability for 3D printing metal components. The Artillery Sidewinder X1 3D Printer is chosen as the printing equipment due to its affordability and compatibility with the research objectives. Finally, the chapter discusses the sample preparation process, which involves modeling the samples using Computer-Aided Design (CAD) software and configuring the printing parameters. The printing parameters for two sets of samples with different layer heights are specified, and additional considerations such as spool placement, nozzle selection, and build plate preparation are outlined.

CHAPTER FOUR

RESULTS AND ANALYSIS

4.1 INTRODUCTION

This chapter examines and interprets the experimental outcomes obtained from the production and evaluation of metal 3D printed samples using the Fused Deposition Modeling (FDM) method, employing optimized post-processing parameters. The copper composite filaments were utilized to fabricate the samples, which were subsequently subjected to debinding and sintering at various holding temperatures. The aim was to investigate and discuss the impact of post-processing parameters on the mechanical and chemical properties of the samples. The chapter begins by describing the parameters that influence the experimental printing setup for metal 3D printed samples using the FDM method. It outlines the optimized design of experiments, highlighting the results obtained through responses and data analysis employing the Taguchi method. Furthermore, the chapter delves into the results obtained after the post-processing steps, such as debinding and sintering, while also comparing the differences between the original copper material and the 3D printed copper polymer composite. Moreover, the chapter presents an analysis of the mechanical properties, including shrinkage and hardness tests, and subsequently examines the microstructure and chemical composition of the samples. The main findings of this study are summarized and compared with existing literature. Additionally, the chapter addresses the limitations and challenges encountered during the fabrication and characterization of the samples using FDM. Finally, potential avenues for future research are suggested.

4.2 PARAMETERS AFFECTING THE EXPERIMENTAL PRINTING SETUP

The first aspect discussed in this chapter is the parameters that influenced the experimental printing setup. Several factors impacted the overall printing process, including the condition of the filament, the 3D printer used, and the adhesion properties of the print bed.

4.2.1 Impact of Filament Condition

The condition of the filament had a notable impact on the results. Upon receiving the filament, it was observed that certain portions were damaged or broken. This necessitated manual intervention during filament loading, potentially introducing inconsistencies in filament feed and affecting the printing process. It is essential to recognize that this inherent limitation of the filament material played a significant role in the observed results.

4.2.2 Printer Selection and Extrusion Process

The choice of the Artillery Sidewinder X1 3D printer with a direct extruder design influenced the outcomes positively. The direct extruder design allowed for convenient filament loading and minimized additional stresses on the filament during printing. This choice contributed to the successful printing of most samples.

Figure 4.1 Illustrates the damaged part of the copper composite filament

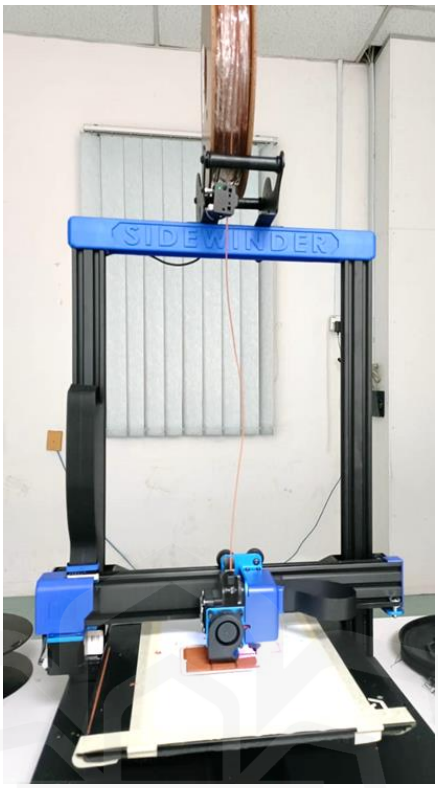

Figure 4.2 Shows the copper filament spool placement on a direct extruder 3D printer

4.2.3 Adhesion properties of the print bed

The adhesion properties of the print bed presented challenges during the experiment. Printed samples adhered tightly to the bed, making removal difficult and leading to some wasted samples. The use of a removable base material, consisting of paper affixed with paper tape, was employed to address this issue. However, it is worth noting that the paper tended to stick to the samples, necessitating additional surface finishing.

4.2.4 Quality evaluation of printed samples after 3D printing

One of the primary outcomes of this study is the quality evaluation and success rate of the printed samples. The majority of the printed samples demonstrated high quality, meeting the desired specifications. However, it's crucial to note that two samples experienced printing failures. These failures were primarily attributed to the fragility of

the copper-polymer composite filament and the limitations of the chosen 3D printer's direct feeding extruder.

4.3 RESULTS BASED ON THE DESIGN OF EXPERIMENTS

The results and discussion chapter presents the findings obtained through the application of the Taguchi method for optimization in the experiment involving debinding and sintering holding times for 3D printed copper-polymer composite samples.

The experimental design consisted of eight samples, divided into two groups based on the layer thickness used for printing (0.3mm and 0.4mm). An L8 orthogonal test array was constructed to determine the optimized parameters for the experiment. The test array represented different combinations of debinding holding time, sintering holding time, and layer thickness. The effects of these parameter combinations on the properties and characteristics of the samples were assessed.

4.3.1 Taguchi method

Table 4.1 Test data summary for responses

Sample No.	**Holding time (hours) (Debinding)**	**Holding time (hours) (Sintering)**	**Layer Thickness (mm)**	**Shrinkage Test (%)**
A	2	3	0.3	40.4944
B	2	3	0.4	40.4944
C	2	5	0.3	43.9900
D	2	5	0.4	N/A
E	4	3	0.3	32.2880
F	4	3	0.4	25.4800

G	4	5	0.3	30.5900
H	4	5	0.4	N/A

Table 4.1 presents the test data summary for the responses, specifically the shrinkage test, for each sample. Each sample is identified by a sample number (A to H) and includes the corresponding values for debinding holding time, sintering holding time, layer thickness, and shrinkage test. The Shrinkage values were calculated by comparing the original measurements of the samples before and after the debinding and sintering processes. The formula for calculating the shrinkage values in percentage is given below,

Shrinkage (%) = [(Initial Dimension – Final Dimension) / Initial Dimension] x 100

4.3.2 Data Analysis

Table 4.2 Response Table for Signal to Noise Ratios

Level	**Debinding**	**Sintering**	**Layer Thickness**
1	33.54	30.65	31.23
2	25.92	28.82	28.24
Delta	7.62	1.83	2.99
Rank	1	3	2

4.3.3 Shrinkage Test versus Debinding, Sintering, and Layer Thickness

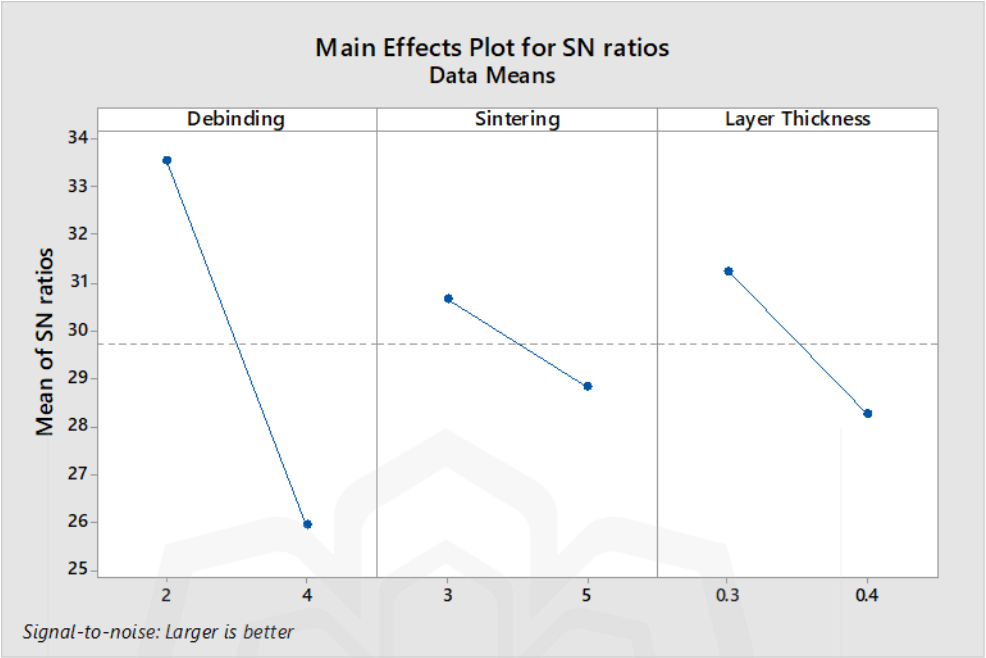

Figure 4.3 Main Effects Plot for Signal to Noise Ratio

To further analyze the data, signal-to-noise ratios (SNR) were calculated for each combination of factors. SNR is used to evaluate the effects of different factors on the response variable. Table 4.2 shows the response table for SNR, with values for each level of debinding, sintering, and layer thickness. The differences (delta) between the SNR values of different levels are calculated, and ranks are assigned based on the magnitude of these differences.

From the SNR response table, we can observe that the highest SNR values for debinding are achieved at Level 1 (33.54) compared to Level 2 (25.92). Therefore, Level 1 is ranked higher (Rank 1) for debinding. For sintering, Level 2 has a slightly higher SNR value (37.87) compared to Level 1 (34.69). Therefore, Level 2 is ranked higher (Rank 2) for sintering. Regarding layer thickness, Level 1 (36.84) has a higher SNR value compared to Level 2 (35.72). Therefore, Level 1 is ranked higher (Rank 1) for layer thickness.

Figure 4.2 represents the main effects plot for SNR, which visualizes the effects of debinding, sintering, and layer thickness on the shrinkage test. From the plot, we can observe the relative importance of each factor in influencing the shrinkage test response variable.

Table 4.3 Response Table for Means

Level	**Debinding (%)**	**Sintering (%)**	**Layer Thickness (%)**
1	48.95	34.69	36.84
2	23.61	37.87	35.72
Delta	25.34	3.18	1.12
Rank	1	2	3

Additionally, the response Table 4.3 for means presents the mean values for each level of debinding, sintering, and layer thickness. The differences (delta) between the mean values of different levels are calculated, and ranks are assigned based on the magnitude of these differences. From the mean response table, we can observe the following: The highest mean value for debinding is achieved at Level 1 (48.95) compared to Level 2 (23.61). Therefore, Level 1 is ranked higher (Rank 1) for debinding. For sintering, Level 1 has a slightly higher mean value (34.69) compared to Level 2 (37.87). Therefore, Level 1 is ranked higher (Rank 1) for sintering. Regarding layer thickness, Level 1 (36.84) has a higher mean value compared to Level 2 (35.72). Therefore, Level 1 is ranked higher (Rank 1) for layer thickness.

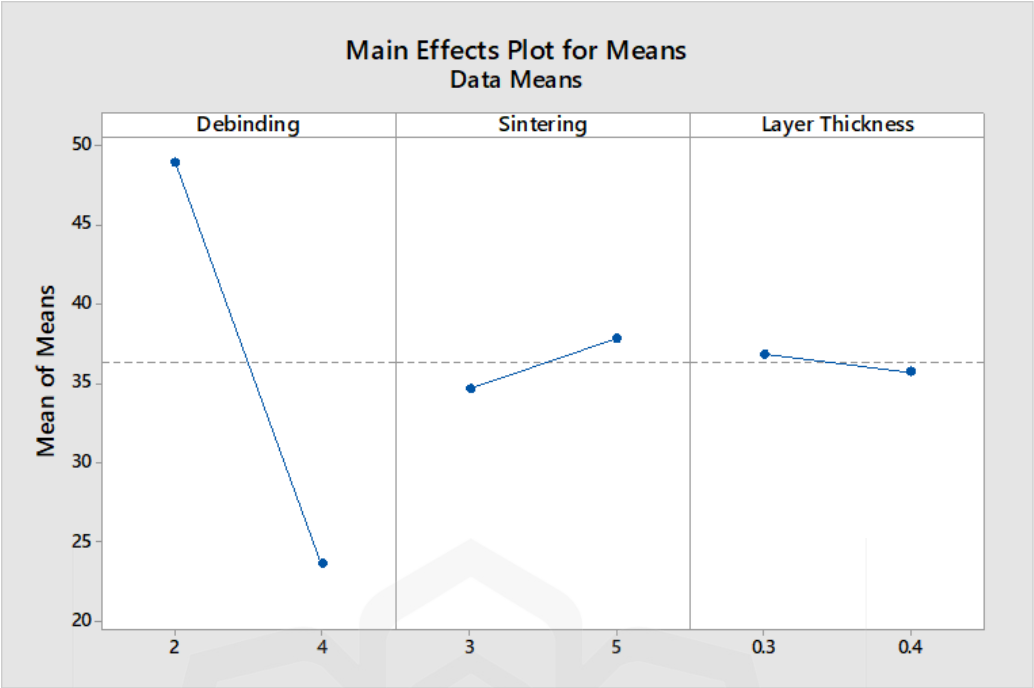

Figure 4.4 Main Effects Plot for Means

Figure 4.3 represents the main effects plot for means, which illustrates the effects of debinding, sintering, and layer thickness on the shrinkage test means. The plot provides insights into the average response values and how they vary with different factor levels. Based on the analysis of the data, the rankings of the factors are as follows: For SNR: debinding (Rank 1), layer thickness (Rank 2), and sintering (Rank 3). For means: debinding (Rank 1), sintering (Rank 2), and layer thickness (Rank 3).

In conclusion, the results and discussion section provide an overview of the experimental findings, highlighting the effects of debinding, sintering, and layer thickness on the shrinkage of 3D-printed copper-polymer composite samples. The Taguchi method was used to optimize the holding temperature for post-processing of FDM-printed metal parts in the debinding and sintering process with different layer thicknesses. The optimized holding temperature was found to be 4 hours for debinding and 5 hours for sintering with a layer thickness of 0.4 mm. Figure 4.6(f) shows that sample F was perfectly debinded and sintered without losing its shape. The microstructure of sample F, shown in Figure 4.12, illustrates the highest amount of atomic diffusion between copper metal particles and the chemical composition of 79.9% copper content, as shown in Table 4.11. These results indicate that the best and

optimized holding time is 4 hours for debinding and 5 hours for sintering with a layer thickness of 0.4 mm.

4.4 POST PROCESSING

Post-processing plays a crucial role in the optimization of 3D printed copper-polymer composite samples. It involves two key steps: debinding and sintering, which are essential for achieving the desired material properties and final product quality.

4.4.1 Debinding

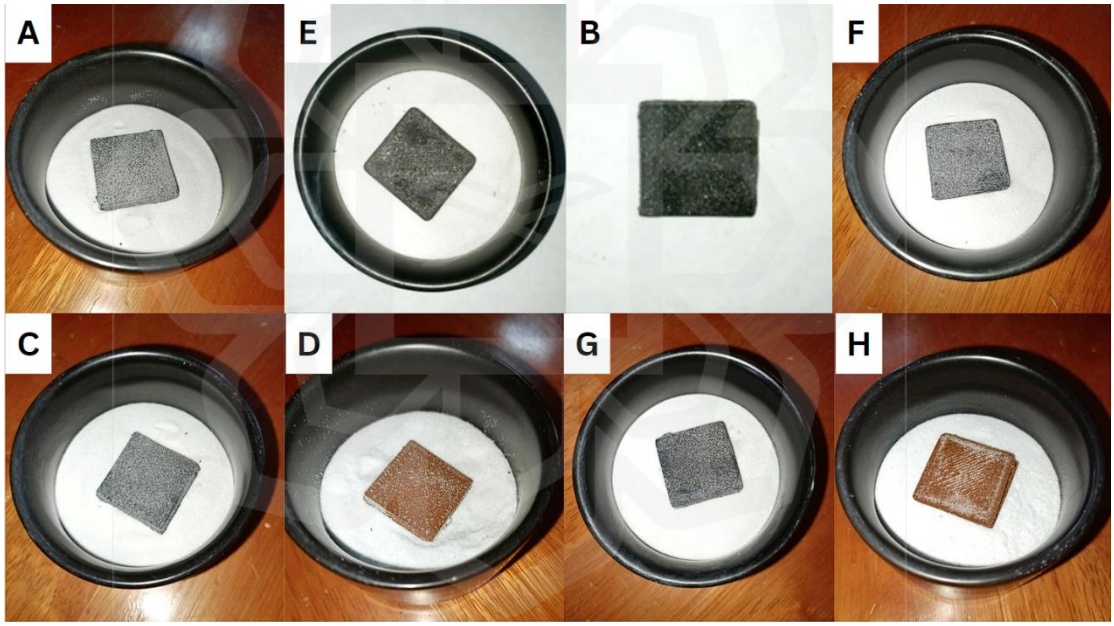

Figure 4.5 Images of samples after Debinding process

During the debinding process, the samples undergo the removal of the polymer binder, leaving behind the copper component. In the experiment, the samples were labeled A to H, with varying debinding and sintering conditions. Four samples, namely A, E, B, and F, underwent longer holding times and were subjected to four debinding temperatures.

The results showed that these samples were successfully debinded. However, samples C, D, G, and H, which had shorter holding times and only two debinding temperatures, displayed suboptimal debinding results. In fact, samples D and H exhibited limited progress in debinding, with only 20 percent completion as shown in Figure 4.4 (D) and (H). This indicated that the faster debinding process was unable to fully remove the polymer binder, resulting in incomplete debinding. These findings highlight the importance of selecting appropriate debinding parameters, particularly longer holding times and a wider range of debinding temperatures, to ensure the complete removal of the polymer binder from the samples. Such a careful approach can only minimize the risk of material waste and enhance the overall quality of the final product.

4.4.2 Sintering

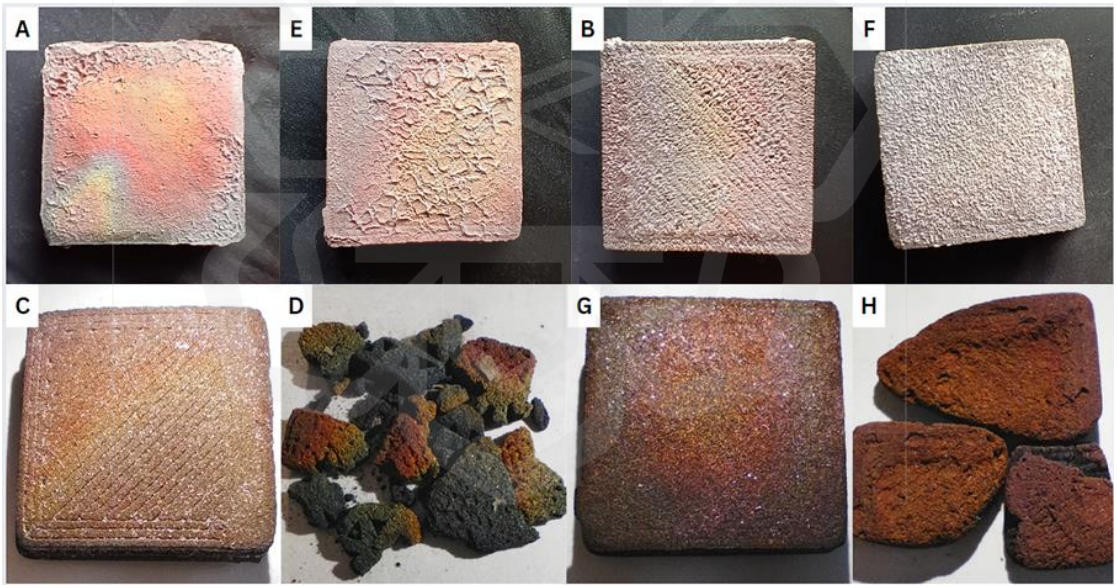

Figure 4.6 Images of samples after Sintering process

Sintering is the process of heating the debinded samples to a high temperature, causing the copper particles to fuse together specifically up to 1050°C and form a solid structure. In the experiment, the sintering stage involved applying 5 different

temperatures ramping up to the samples based on the design of experiments using Taguchi method.

Among the samples, A, E, B, and F, which underwent longer holding times and a wider range of sintering temperatures, achieved successful sintering as shown in Figure 4.5 (A), (E), (B) and (F). However, samples C, D, G, and H, with shorter holding times and only three sintering temperatures, exhibited varied sintering outcomes. Samples C and G were effectively sintered, while samples D and H showed no sintering progress instead sample D looks like powder and few broken pieces because this sample was so brittle that it broke into pieces while holding in hands, and in case of sample H this sample was very soft like a clay material after sintering process as shown in Figure 4.5. (D) and (H). This suggests that the shorter sintering duration and limited temperature range hindered the complete sintering of the samples. To optimize the sintering process, it is crucial to employ longer holding times and a broader range of sintering temperatures. This approach ensures the adequate fusion of copper particles, resulting in a strong and well-consolidated final product.

Overall, the experimental results demonstrate that achieving optimal debinding and sintering conditions is vital for post-processing the 3D printed copper-polymer composite samples. Longer holding times and wider temperature ranges were found to be more effective in ensuring complete debinding and sintering, thereby enhancing the quality and reliability of the final products.

4.4.3 Finished sample

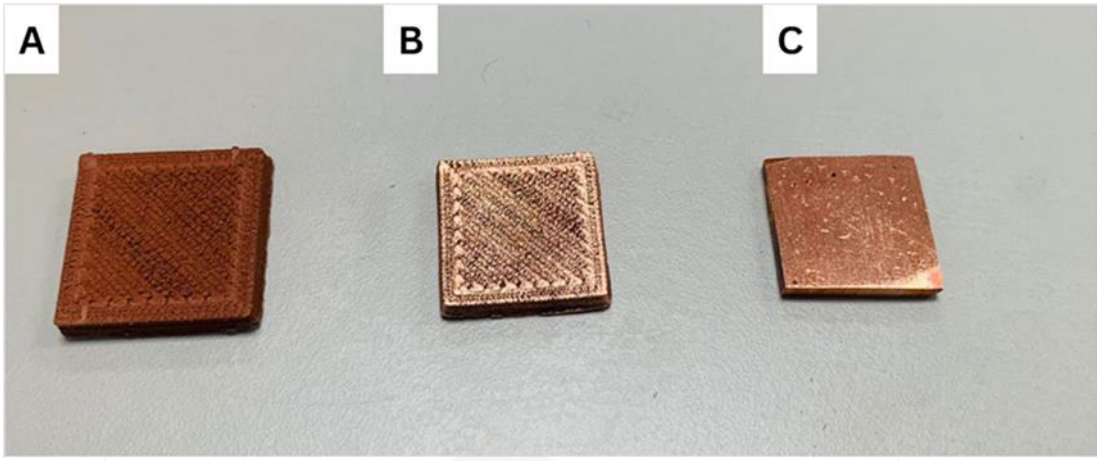

Figure 4.7 Samples before and after sintering, polishing and surface finishing; (A). The 3D printed sample in its green state, (B). The top view of the processed sample, (C). The bottom view of the processed sample

After 3D printing the sample, it will be in green state as shown in Figure.4.6 (A), The samples then underwent post Sintering, which included polishing and surface finishing. They were sanded with various grits of sandpaper and polished to make them smooth and shiny. Other surface treatments may have been used as well. The samples were carefully checked to ensure they met the quality standards. The polishing and surface finishing of the samples improved their appearance as shown in Figure 4.6. (B) and (C). They also reduced the surface roughness and porosity of the sintered metal parts, which are common challenges in 3D printing.

4.5 MECHANICAL PROPERTIES ANALYSIS

The mechanical properties of the 3D printed metal samples were evaluated using two tests: Shrinkage test and Vickers hardness test.

4.5.1 Shrinkage value measurements and analysis

The shrinkage values were measured using Vernier calliper, micrometre, and a mini electronic precision scale to determine the dimensional changes in the samples after the debinding and sintering process. The measurements were taken in the x, y, and z axes.

4.5.1.1 Vernier calliper measurements

In the case of Samples D and H in Vernier Calliper measurements, only the weight measurements were recorded, and no data could be measured for the dimensions on the X-axis and Y-axis because the samples were converted into pieces. It was observed that Sample B exhibited the least shrinkage in both the X and Y axes, while Sample C displayed the highest shrinkage among all the samples, as indicated in Table 4.4.

Table 4.4 Vernier Calliper measurements

Sample	**X-axis (mm)**	**Y-axis (mm)**
A	22.9	23.1
B	23.1	23.0
C	22.0	21.5
D	The sample got completely shattered, leaving us with only the option to measure its weight and no way to determine its size.	
E	23.0	23.0
F	23.0	22.5
G	23.1	22.9
H	The sample got completely shattered, leaving us with only the option to measure its weight and no way to determine its size.	

4.5.1.2 Micrometre measurements

For Samples D and H, only the weight measurements were recorded in micrometres. Unfortunately, no data could be obtained for the dimensions along the Z-axis as the samples were converted into pieces. Notably, Samples A and F demonstrated the least shrinkage in the Z-axis, while Sample B exhibited the highest shrinkage among all the samples, as shown in Table 4.5.

Table 4.5 Micrometer measurements

Sample	**Z-axis (mm)**
A	4.5
B	3.5
C	3.7
D	The sample got completely shattered, leaving us with only the option to measure its weight and no way to determine its size.
E	4.0
F	4.5
G	4.1
H	The sample got completely shattered, leaving us with only the option to measure its weight and no way to determine its size.

4.5.1.3 Weight Machine

The weights of the samples measured using the mini electronic precision scale also provide information about the changes in mass due to the debinding and sintering process. Sample D and H were already shattered into small pieces and the shrinkage value couldn’t be measured. The sample G exhibit the lowest shrinkage in terms of weight, while the sample A showed the highest shrinkage as shown in Table 4.6.

Table 4.6 Weight measurements

Sample	Weight (grams)
A	9.4
B	9.7
C	9.5
D	3.0
E	10.5
F	10.5
G	10.6
H	8.9

In conclusion, when considering all the measurements, including weight, height, length, and width of the samples from Table 4.4, 4.5 and 4.6, it becomes evident that sample C exhibited the most significant shrinkage, while sample F displayed the least shrinkage.

4.5.2 Vickers hardness test results and analysis

The Vickers hardness test was performed to evaluate the hardness properties of the printed metal samples. This test provided an indication of the hardness properties of the printed metal samples. From the obtained results from Table 4.7, it can be observed that samples A, E, and F exhibit higher hardness values compared to samples B, and C. This difference in hardness may be attributed to variations in the composition or sintering conditions of the copper-polymer composite filament used for each sample. Sample D and H, which turned into powder and could not be tested, indicates a failure in the printing process.

Table 4.7 Hardness test results

Sample	Mean Hardness (HV2)
A	2165.73
B	1910.58
C	1929.07
D	The sample got completely shattered, leaving us with only the option to measure its weight and no way to determine its size.
E	2116.73
F	2269.34
G	2076.74
H	The sample got completely shattered, leaving us with only the option to measure its weight and no way to determine its size.

Overall, the results of the mechanical properties analysis highlight the variations in dimensional changes and hardness properties among the printed metal samples. These variations may be influenced by factors such as the composition of the filament, debinding and sintering conditions, and printing process parameters. Further investigation and optimization are recommended to ensure consistent and desired mechanical properties in future prints.

4.5.3 Scanning electron microscopy analysis of microstructure

SEM analysis revealed that prior to the debinding and sintering process, all the 3D printed samples displayed a consistent microstructure. As depicted in Figure 4.7, the microstructure exhibited metal powder particles arranged as granules with a loose configuration. Surrounding these granules was a binding agent composed of polymer materials. This microstructure represents the pre-processed state of the 3D printed samples.

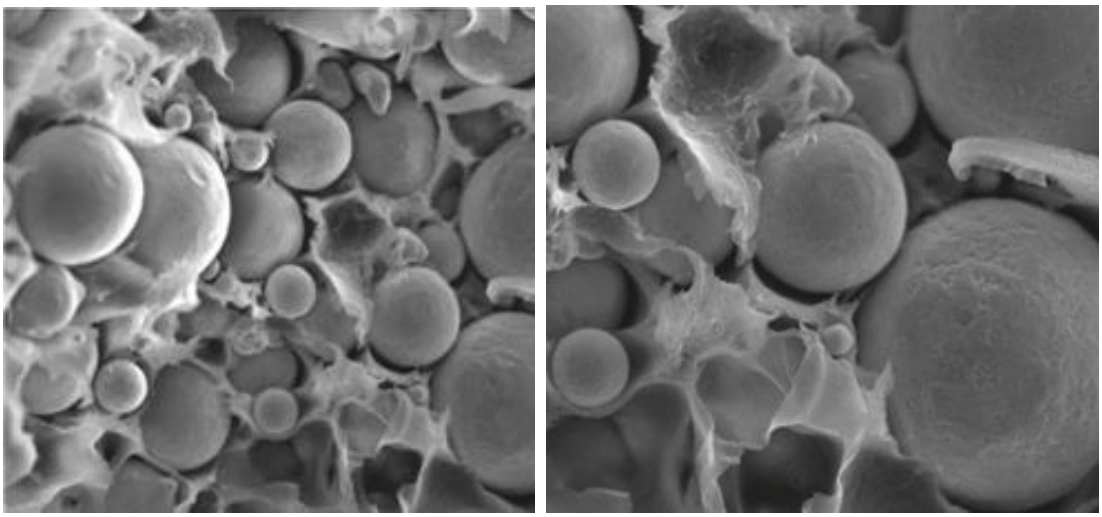

Figure 4.8 Microstructure of Samples before debinding and sintering processes

Sample A

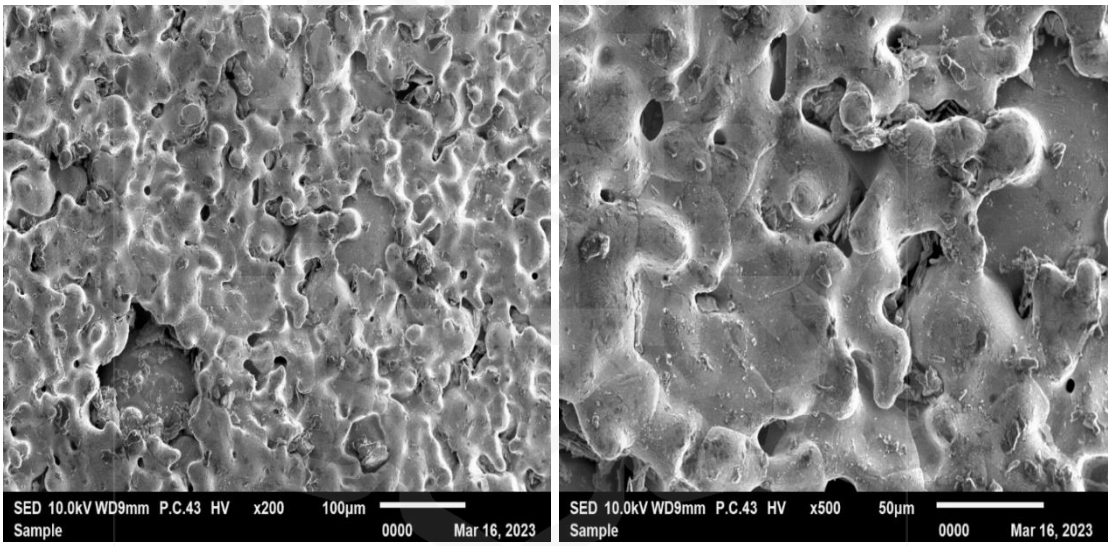

Figure 4.9 SEM images of Sample A 3D printed at 0.3-layer thickness

Sample E

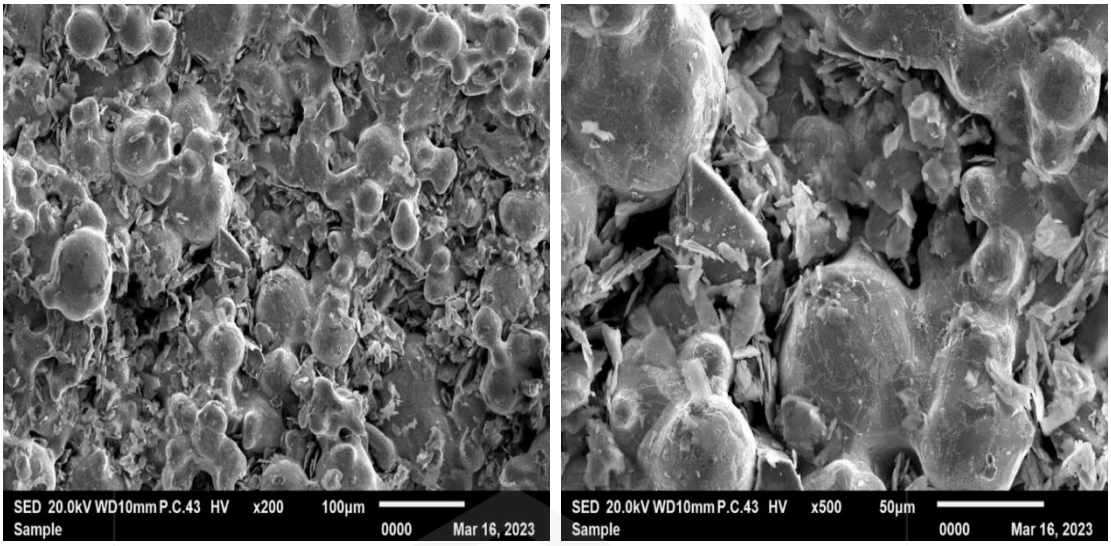

Figure 4.10 SEM images of Sample E 3D printed at 0.4-layer thickness

Sample B:

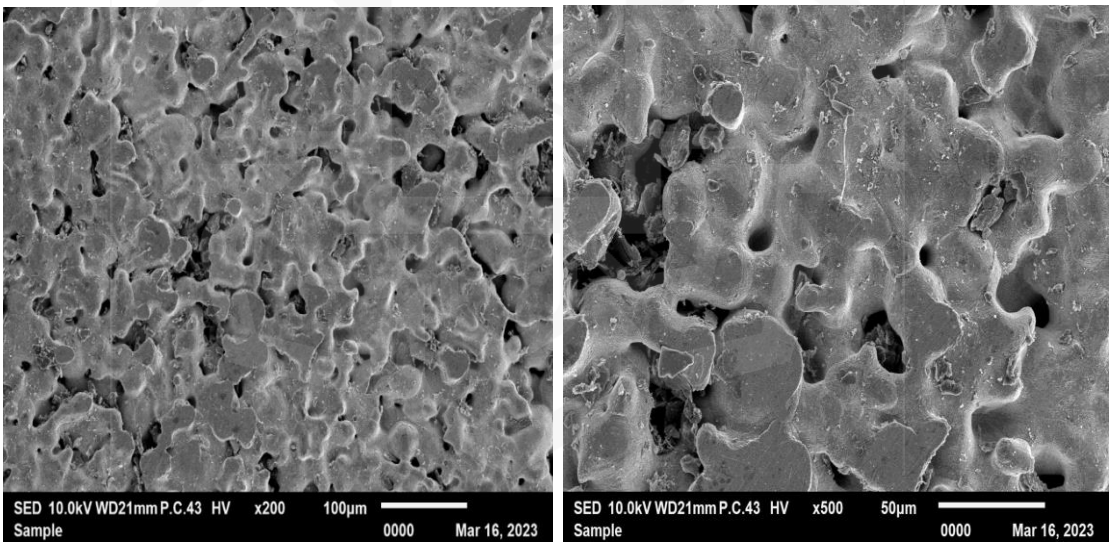

Figure 4.11 SEM images of Sample B 3D printed at 0.3-layer thickness

Sample F:

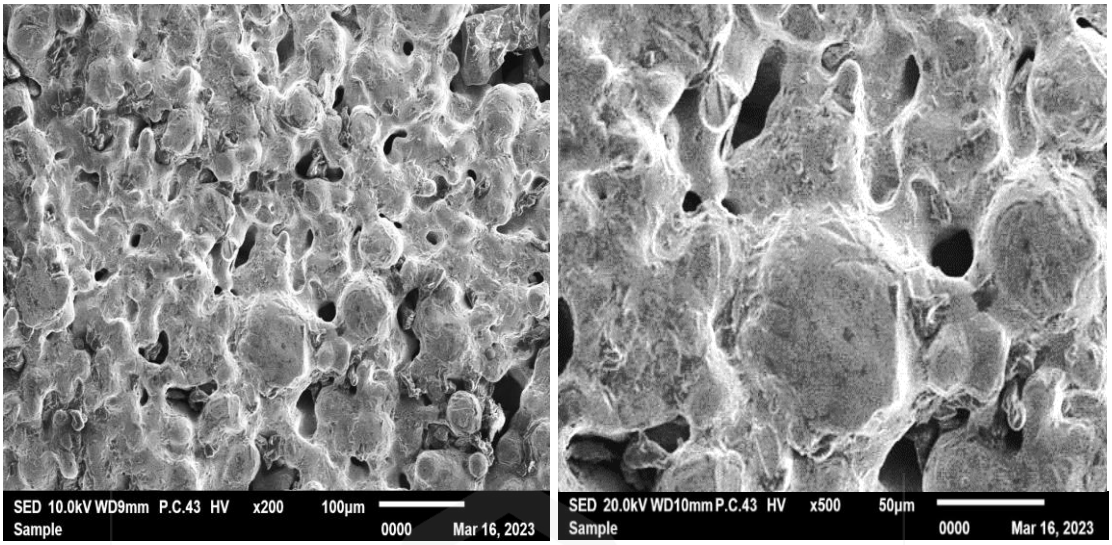

Figure 4.12 SEM images of Sample F 3D printed at 0.4-layer thickness

After subjecting samples, A, E, B, and F to the Sintering process in Furnace 1, with a holding time of 5 hours at a temperature of 1050 degrees Celsius, the copper particles achieved a bonding rate of up to 70%. These samples were 3D printed with a specific layer thickness of 0.3 mm. However, there were variations observed among these samples in terms of microstructure, indicating that the atomic motion within the copper particles and the diffusion ability between them differed. These variations ultimately impacted the quality of the sintered parts.

Upon analysing samples, A, B, and F (as depicted in Figures 4.8, 4.10, and 4.11 respectively), it was evident that the atomic diffusion was exceptional. Although some surface pores were still visible in these samples, the absence of polymer traces within the microstructure was a positive outcome. The presence of polymer binders in the sintered parts can compromise their strength, and therefore, the absence of such traces indicates that the parts are likely to possess optimal strength. However, sample E (shown in Figure 4.9) exhibited numerous irregular small grains that did not diffuse adequately, accompanied by the presence of polymer traces and remaining pores. This outcome can be attributed to uneven heat distribution during the sintering process within the furnace.

Sample C:

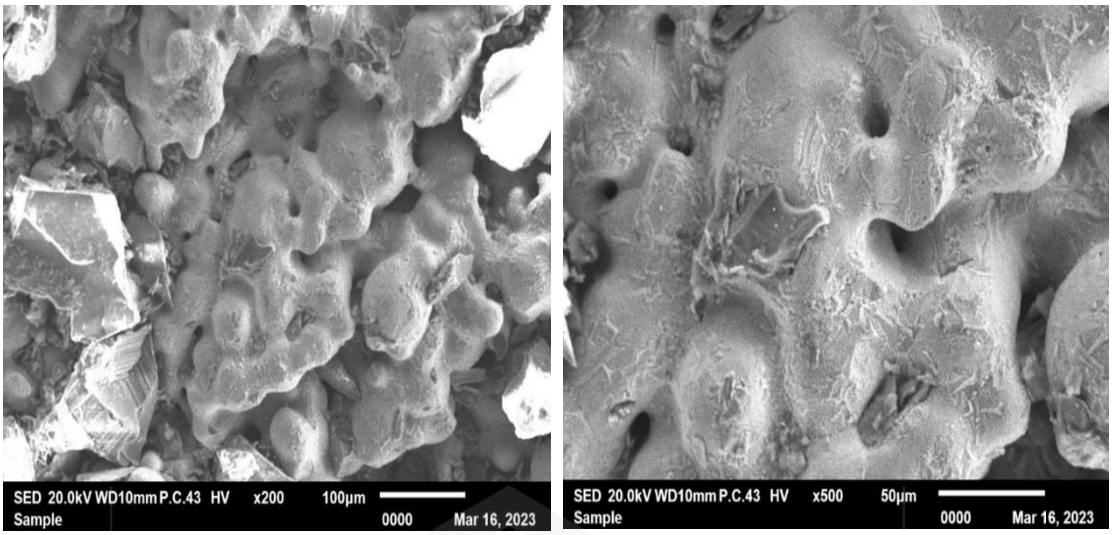

Figure 4.13 SEM images of Sample C 3D printed at 0.3-layer thickness

Sample G:

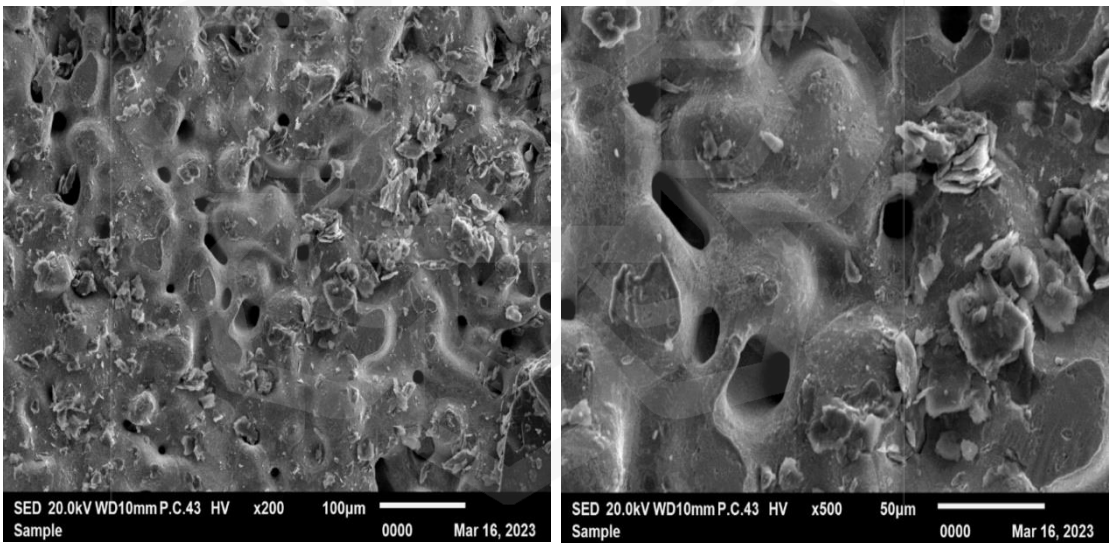

Figure 4.14 SEM images of Sample G 3D printed at 0.4-layer thickness

After the sintering process of Samples C, D, G, and H the samples which were properly sintered were sample C and sample G, and other two samples that is sample D and sample H were not completely sintered infact they remained as if they were only debinded not sintered, in terms of their physical characteristics because as shown in Figure 4.5, sample D looks like few broken pieces because this sample was so brittle that it broke into pieces while holding in hands, and in case of sample H this sample

was very soft like a clay material after sintering process. Hence these samples couldn't be taken for SEM anlaysis. The incomplete debinding of samples D and H can be attributed to a single crucial factor: insufficient holding time in the furnace. Upon evaluation, it became evident that, initially, samples D and H were placed in furnace 1, which was prematurely shut down due to technical issues. This resulted in a significantly reduced holding time, and it is this limited holding time that primarily accounts for the incomplete debinding of these two samples. It became clear that the holding time emerged as the singular and paramount factor influencing the sample outcome.

After sintering process of sample C in Figure 4.12 it was Subjected to SEM analysis and the microstructure showed that the grains were tightly packed and some were binded but still the pores remained the same while in case of sample G Figure 4.13 shows the SEM images of sample G and it showed a significant amount of diffusion between the copper particles and still the pores are not filled yet. This is the result of incomplete sintering.

In conclusion the author says that the samples which were debinded and sintered for longer time in case of Sample A, E, B, and F in Furnace 1 setting, they exhibited the same kind of results in Furnace 2 like the samples C and G, as they were debinded and sintered for lesser time and yet converted into a completed sintered sample like the samples A, E, B and F and excluding the other two samples that are sample D and H as they couldn't be sintered in Furnace 2 setting and after all there is a very important thing to note here that using the faster debinding and sintering time could lead to an incomplete sintered sample some times which is why it is better to hold the sample for longer time for better results. As the researchers cannot take risk while decreasing the holding times.

4.5.4 Energy Dispersive X-Ray Spectroscopy (EDX) analysis for chemical composition

The EDX analysis was conducted to determine the chemical composition of the printed metal samples (A, E, B, F, C, and G) and compare them to the expected composition of

the copper-polymer composite filament used for printing. The results of the analysis provide valuable insights into the elemental compositions and any deviations or impurities detected in the samples.

Table 4.8 Chemical Composition of 3D printed Copper composite for sample A.

Element	Weight %	Standard Deviation
Cu	78.4	1.2
O	20.3	1.1
Ca	1.4	0.4

Sample A exhibited a composition with 78.4% copper (Cu), 20.3% oxygen (O), and 1.4% calcium (Ca) as shown in Table 4.8. The copper content aligns with the expected composition, indicating the successful use of the copper-polymer composite filament. However, the slightly higher oxygen content suggests the presence of oxide layers on the sample's surface or incomplete sintering. Additionally, the presence of calcium may indicate a contamination or impurity in the filament or during the printing process.

Table 4.9 Chemical Composition of 3D printed Copper composite for sample E

Element	Weight %	Standard Deviation
Cu	55.0	0.6
O	28.6	0.5
Mg	7.7	0.3

In Sample E, the elemental composition revealed a significant deviation from the expected values. It consisted of 55.0% copper (Cu), 28.6% oxygen (O), 7.7% magnesium (Mg) as shown in Table 4.9. The lower copper content indicates a departure

from the intended composition, which could be attributed to incomplete mixing of the copper-polymer composite or issues during the printing process. The higher oxygen content suggests the presence of oxide layers or incomplete sintering. Moreover, the presence of magnesium and silicon points towards impurities or contaminants present in the filament or the printing environment.

Table 4.10 Chemical Composition of 3D printed Copper composite for sample B

Element	Weight %	Standard Deviation
Cu	74.2	0.4
O	21.9	0.3
Mg	1.8	0.2
Ca	0.4	0.1

For Sample B, the composition included 74.2% copper (Cu), 21.9% oxygen (O), 1.8% magnesium (Mg), and 0.4% calcium (Ca) as shown in Table 4.10. The copper content is relatively close to the expected composition, indicating successful printing with the copper-polymer composite filament. However, the slightly higher oxygen content suggests the presence of oxide layers or incomplete sintering. The presence of magnesium, silicon, and calcium indicates potential impurities or contaminants originating from the filament or the printing environment.

Table 4.11 Chemical Composition of 3D printed Copper composite for sample F

Element	Weight %	Standard Deviation
Cu	79.9	2.7
O	20.1	2.7

Sample F demonstrated a composition comprising 79.9% copper (Cu) and 20.1% oxygen (O) as shown in Table 4.11. The copper content aligns with the expected composition, indicating successful printing using the copper-polymer composite filament. Similarly, the slightly higher oxygen content suggests the presence of oxide layers or incomplete sintering.

Table 4.12 Chemical Composition of 3D printed Copper composite for sample C

Element	Weight %	Standard Deviation
Cu	67.1	1.7
O	25.1	1.4
S	1.5	0.4

In Sample C, the composition included 67.1% copper (Cu) and 25.1% oxygen (O) as shown in Table 4.12. The copper content is relatively close to the expected composition, indicating successful printing with the copper-polymer composite filament. However, the higher oxygen content suggests the presence of oxide layers or incomplete sintering.

Table 4.13 Chemical Composition of 3D printed Copper composite for sample G

Element	Weight %	Standard Deviation
Cu	50.1	2.8
O	30.1	2.2
Mg	5.3	1.3

Sample G exhibited a composition comprising 50.1% copper (Cu), 30.1% oxygen (O), and 5.3% magnesium (Mg) as shown in Table 4.13. The lower copper content in Sample G indicates a departure from the intended composition. The higher oxygen content suggests the presence of oxide layers or incomplete sintering. The presence of magnesium indicates a potential impurity or contamination originating from

the filament or the printing environment. Interpreting these findings in light of the research objectives and implications for the quality and performance of the printed metal samples, the observed deviations in elemental compositions can have significant effects.

A lower copper content, as seen in Sample E and Sample G, may result in reduced strength and conductivity, as copper is the primary reinforcing phase, while the higher copper content in Sample A and Sample F, may result in the higher strength and conductivity of the samples. The presence of impurities, incomplete sintering, or contaminants can alter the microstructure of the printed metal, leading to voids, inclusions, or weakened interfaces that compromise the overall integrity and properties of the samples.

In conclusion, the EDX analysis provides valuable insights into the elemental compositions and potential deviations in the printed metal samples compared to the expected composition of the copper-polymer composite filament. The presence of impurities, incomplete sintering, or contaminants may impact the mechanical properties and microstructure.

4.6 CHAPTER SUMMARY

The fourth chapter of the study focuses on the results and analysis of the experiments conducted on metal 3D printed samples using the Fused Deposition Modelling (FDM) method. The chapter begins by introducing the purpose of the study, which is to investigate the impact of post-processing parameters on the mechanical and chemical properties of the samples. It highlights the use of copper composite filaments and the subsequent debinding and sintering processes. The chapter discusses the parameters that affect the experimental printing setup, including the condition of the filament, the 3D printer used, and the adhesion properties of the print bed. It emphasizes the need for careful handling of fragile filaments and describes the selection of the Artillery Sidewinder X1 3D printer for its direct extruder design. The challenges related to print bed adhesion are addressed, and the use of a removable base material is mentioned.

The chapter then delves into the results obtained from the experiments, which employed the Taguchi method for optimization. The design of experiments included different combinations of debinding holding time, sintering holding time, and layer thickness. The effects of these parameters on the mechanical properties of the samples were analysed. The results are presented in tables and discussed in terms of shrinkage values, hardness tests, and microstructure analysis. Shrinkage measurements were taken in the x, y, and z axes using Vernier callipers, micrometres, and a mini electronic precision scale. The results showed variations in shrinkage values among the samples, with different dimensional changes observed. Vickers hardness tests were performed to evaluate the hardness properties of the samples, indicating variations in hardness values. Microstructure analysis using scanning electron microscopy (SEM) provided insights into the pre-processed state of the samples, as well as their microstructure after debinding and sintering. The analysis revealed differences in atomic diffusion and bonding rates among the samples, with some exhibiting successful sintering and others showing incomplete or failed sintering.

The chapter also includes an analysis of the chemical composition of the samples using energy-dispersive X-ray spectroscopy (EDX). The results showed variations in the elemental compositions compared to the expected composition of the copper-polymer composite filament. These variations may affect the mechanical properties and overall quality of the samples. Throughout the chapter, the findings are compared with existing literature, limitations and challenges encountered during the fabrication and characterization processes are discussed, and potential avenues for future research are suggested.

CHAPTER FIVE

CONCLUSION AND RECOMMENDATIONS

5.1 CONCLUSION

The research has successfully achieved its proposed objectives, involving the fabrication of a Copper polymer composite using the fused deposition modeling technique. Furthermore, the post-processing of the copper composite sample was successfully converted into 90% pure metal, by removing the binder and diffusing the metal particles with two processes, debinding and sintering respectively. The key conclusions from the study include: The 3D printing of the copper polymer composite filament was influenced by various factors like to ensure a proper extrusion of the copper composite filament, a 0.6 mm diameter nozzle made of hardened steel was used, while caution was required during spool placement to avoid pull and friction. Additionally, it was necessary to prepare the build plate properly to prevent prints from welding onto it, especially when using metal polymer composite filaments. The research utilized a low-cost Fused Deposition Modelling (FDM) 3D printer worth $350, which was significantly more affordable compared to a powder bed fusion metal 3D printer costing around $400,000. This achievement demonstrates the successful printing of metal using a cost-effective FDM 3D printer.

The post-processing of the printed samples played a crucial role in converting the copper polymer composite into pure metal. The copper metal part contained 79% copper, while the remaining portion consisted of other minerals such as oxygen, magnesium, calcium, etc. This outcome was considered a significant achievement.

The parameters for post-processing, determined through the Taguchi method and design of experiments, were found to be significant. It was observed that a slow debinding process was necessary to prevent warping and shape destruction of the metal due to the polymer material. Similarly, longer holding times during sintering were preferred to ensure proper sintering and maintain the shape of the metal. The post-processed metals exhibited a 40% shrinkage, and the samples demonstrated acceptable

hardness up to 2kg. The microstructure displayed a moderate amount of diffusion with minimal holes, and the chemical composition indicated a significant copper content in the final samples. However, two samples subjected to shorter holding times during debinding and sintering were found to be soft and brittle, resulting in destruction.

5.2 RECOMMENDATION

Further research is needed to optimize post-processing parameters for achieving desired purity and mechanical properties in 3D printed metal parts. Experiment with alternative debinding and sintering techniques to improve efficiency, cost-effectiveness, and part quality. Streamline post-processing steps to make metal FDM 3D printing more cost-effective and accessible. Overcome size limitations by exploring technologies like microwave sintering for faster processing times. Promote metal FDM 3D printing in smaller industries, highlighting its cost-effectiveness and potential applications.

Consider future directions such as material development, multi-material printing, design optimization, in-situ monitoring, customized medical implants, rapid prototyping, tooling production, and sustainability practices to drive innovation and impact various industries.

REFERENCES

All3DP, A. (2021, March 18). *FDM Metal 3D Printing*.

Ambrus, G. G., Eick, C. M., Kaiser, D., & Kovács, G. (2021). Getting to Know You: Emerging Neural Representations during Face Familiarization. *The Journal of Neuroscience*, *41*(26), 5687–5698.

Baufeld, B., Brandl, E., & van der Biest, O. (2011). Wire based additive layer manufacturing: Comparison of microstructure and mechanical properties of Ti–6Al–4V components fabricated by laser-beam deposition and shaped metal deposition. *Journal of Materials Processing Technology*, *211*(6), 1146–1158.

Brad Woods. (n.d.). *The Virtual Foundry, inc. – FFF/Bound Metal 3D Printing in the Lab*. Retrieved June 25, 2023,

Calì, M., Pascoletti, G., Gaeta, M., Milazzo, G., & Ambu, R. (2020). New filaments with natural fillers for FDM 3D printing and their applications in biomedical field. *Procedia Manufacturing*, *51*, 698–703.

Chowdhury, S., Yadaiah, N., Prakash, C., Ramakrishna, S., Dixit, S., Gupta, L. R., & Buddhi, D. (2022). Laser powder bed fusion: a state-of-the-art review of the technology, materials, properties & defects, and numerical modelling. *Journal of Materials Research and Technology*, *20*, 2109–2172.

Clemens, F., Schulz, J., Gorjan, L., Liersch, A., Sebastian, T., & Sarraf, F. (2021). Debinding and Sintering of Dense Ceramic Structures Made with Fused Deposition Modeling. In *Industrializing Additive Manufacturing* (pp. 293–303). Springer International Publishing.

Dai, Y. H., & Wang, X. (2019). Design and Verification of a Metal 3D Printing Device Based on Contact Resistance Heating. *Solid State Phenomena*, *298*, 64–68.

Fafenrot, S., Grimmelsmann, N., Wortmann, M., & Ehrmann, A. (2017). Three-dimensional (3D) printing of polymer-metal hybrid materials by fused deposition modeling. *Materials*, *10*(10).

Fu, Z., & Körner, C. (2022). Actual state-of-the-art of electron beam powder bed fusion. *European Journal of Materials*, *2*(1), 54–116.

Gao, W., Zhang, Y., Ramanujan, D., Ramani, K., Chen, Y., Williams, C. B., Wang, C. C. L., Shin, Y. C., Zhang, S., & Zavattieri, P. D. (2015). The status, challenges, and future of additive manufacturing in engineering. *Computer-Aided Design*, *69*, 65–89.

Ghariblu, H., & Rahmati, S. (2014). New Process and Machine for Layered Manufacturing of Metal Parts. *Journal of Manufacturing Science and Engineering*, *136*(4).

Gordeev, E. G., Galushko, A. S., & Ananikov, V. P. (2018). Improvement of quality of 3D printed objects by elimination of microscopic structural defects in fused deposition modeling. *Plos One*, *13*(6), e0198370.

Gupta, A. A. (2023, February 11). *Online 3D Printing Service in India - FDM, SLA, SLS, CNC, & Injection Molding*.

Hao, B., & Lin, G. (2020). 3D Printing Technology and Its Application in Industrial Manufacturing. *IOP Conference Series: Materials Science and Engineering*, *782*(2), 022065.

Huang, R., Dai, N., Pan, C., Yang, Y., Jiang, X., Tian, S., & Zhang, Z. (2023). Grid-tree composite support structures for lattice parts in selective laser melting. *Materials and Design*, *225*.

Hwang, S., Reyes, E. I., Moon, K., Rumpf, R. C., & Kim, N. S. (2015). Thermo-mechanical Characterization of Metal/Polymer Composite Filaments and Printing Parameter Study for Fused Deposition Modeling in the 3D Printing Process. *Journal of Electronic Materials*, *44*(3), 771–777.

Integza. (2021). *How I 3D Printed a Metal Aerospike Rocket at Home*. Youtube.

Jahani, B., Wang, X., & Brooks, A. (2020). Additive Manufacturing Techniques for Fabrication of Bone Scaffolds for Tissue Engineering Applications. *Recent Progress in Materials*, *2*(3), 1–41.

Jandric, Z., Labudovic, M., & Kovacevic, R. (2004). Effect of heat sink on microstructure of three-dimensional parts built by welding-based deposition. *International Journal of Machine Tools and Manufacture*, *44*(7–8), 785–796.

Jeanne Schweder. (2021, July 6). *U.S. Air Force Looks to Fly with 3D Printed Parts*. Automation World.

Karabulut, Y., & Ünal, R. (2022). Additive manufacturing of ceramic particle-reinforced aluminum-based metal matrix composites: a review. *Journal of Materials Science*, *57*(41), 19212–19242.

Kinstlinger, I. S., Bastian, A., Paulsen, S. J., Hwang, D. H., Ta, A. H., Yalacki, D. R., Schmidt, T., & Miller, J. S. (2016). Open-Source Selective Laser Sintering (OpenSLS) of Nylon and Biocompatible Polycaprolactone. *PLOS ONE*, *11*(2), e0147399.

Kristiawan, R. B., Imaduddin, F., Ariawan, D., Ubaidillah, & Arifin, Z. (2021). A review on the fused deposition modeling (FDM) 3D printing: Filament processing, materials, and printing parameters. *Open Engineering*, *11*(1), 639–649.

Kumar Singh, A., & Chauhan, S. (2016). Technique to Enhance FDM 3D Metal Printing. *Bonfring International Journal of Industrial Engineering and Management Science*, *6*(4), 128–134.

Li, J. Z., Alkahari, M. R., Rosli, N. A. B., Hasan, R., Sudin, M. N., & Ramli, F. R. (2019). Review of Wire Arc Additive Manufacturing for 3D Metal Printing. *International Journal of Automation Technology*, *13*(3), 346–353.

Manufactur3d (M.). (2023). 8 Techniques For Post-Processing Of FDM 3D Printed Parts (2023) - Manufactur3D. *Manufactur3D*.

Mechninja (M.). (2021, October 9). *FDM Printing Post Processing and Curing Methods*. TheMechNinja.

Ngo, T. D., Kashani, A., Imbalzano, G., Nguyen, K. T. Q., & Hui, D. (2018). Additive manufacturing (3D printing): A review of materials, methods, applications and challenges. *Composites Part B: Engineering*, *143*, 172–196.

Ni, J., Yu, M., & Han, K. (2018). Debinding and Sintering of an Injection-Moulded Hypereutectic Al–Si Alloy. *Materials*, *11*(5), 807.

Post processing for FDM printed parts | Hubs. (n.d.). Hubs. Retrieved June 26, 2023, from

Rahmatabadi, D., Aminzadeh, A., Aberoumand, M., & Moradi, M. (2021). *Mechanical Characterization of Fused Deposition Modeling (FDM) 3D Printed Parts* (pp. 131–150).

Ramazani, H., & Kami, A. (2022). Metal FDM, a new extrusion-based additive manufacturing technology for manufacturing of metallic parts: a review. *Progress in Additive Manufacturing*, *7*(4), 609–626.

Syam, W. P., Mannan, M. A., & Al-Ahmari, A. M. (2011). Rapid prototyping and rapid manufacturing in medicine and dentistry. *Virtual and Physical Prototyping*, *6*(2), 79–109.

Tamayo, J. A., Riascos, M., Vargas, C. A., & Baena, L. M. (2021). Additive manufacturing of Ti6Al4V alloy via electron beam melting for the development of implants for the biomedical industry. *Heliyon*, *7*(5), e06892.

Tim, T. (n.d.). *Founder of FDM 3D printing technology*. Clever Creations. Retrieved June 25, 2023.

Velásquez-García, L. F., & Kornbluth, Y. (2021). Biomedical Applications of Metal 3D Printing. *Annual Review of Biomedical Engineering*, *23*(1), 307–338.

APPENDIX I

LIST OF PUBLICATIONS

Published and Under Review Journals

- **Iftekar, S. F.,** Aabid, A., Amir, A., & Baig, M. (2023). Advancements and Limitations in 3D Printing Materials and Technologies: A Critical Review. Polymers, 15(11), 2519. Https://doi.org/10.3390/polym15112519 (PUBLISHED)

- **Iftekar, S. F.,** Sukindar, N. A., Amir, A., & Aabid, A. (2023b, May 12). https://www.researchgate.net/publication/370803503,_enhancing_metal_3d_printing_with_fused_deposition_modeling-a_short_review. (PUBLISHED)